An exon-intron split framework to prioritize miRNA-driven post-transcriptional regulatory signals and its application to study energy homeostasis in pigs

Emilio Mármol-Sánchez[1*], Susanna Cirera[2], Laura M. Zingaretti[3], Mette Juul Jacobsen[2], Yuliaxis Ramayo-Caldas[4], Claus B. Jørgensen[2], Merete Fredholm[2], Tainã Figueiredo Cardoso[1†], Raquel Quintanilla[4], Marcel Amills[1,5]

[1]Centre for Research in Agricultural Genomics (CRAG), CSIC-IRTA-UAB-UB, Universitat Autònoma de Barcelona, 08193 Bellaterra, Spain.

[2]Department of Veterinary and Animal Sciences, Faculty of Health and Medical Sciences, University of Copenhagen, 1871 Frederiksberg C, Denmark.

[3]Universidad Nacional de Villa María, Villa María, Córdoba, Argentina.

[4]Animal Breeding and Genetics Program, Institute for Research and Technology in Food and Agriculture (IRTA), Torre Marimon, 08140 Caldes de Montbui, Spain.

[5]Departament de Ciència Animal i dels Aliments, Universitat Autònoma de Barcelona, 08193 Bellaterra, Barcelona, Spain.

*Emilio Mármol-Sánchez current address: Stockholm University, The Wenner-Gren Institute, Department of Molecular Biosciences, SciLifelab.

[†]Tainã Figueiredo Cardoso current address: Embrapa Pecuária Sudeste, Empresa Brasileira de Pesquisa Agropecuária (EMBRAPA), 13560-970, São Carlos, SP, Brazil.

Corresponding author: Emilio Mármol-Sánchez. Stockholm University, The Wenner-Gren Institute, Department of Molecular Biosciences, SciLifelab. Email: emilio.marmol.sanchez@gmail.com

Abstract

Bulk sequencing of RNA transcripts has typically been used to quantify gene expression levels and regulatory signals in different experimental systems. However, linking differentially expressed (DE) mRNA transcripts to gene expression regulators, such as miRNAs, remains challenging, as miRNA-mRNA interactions are commonly identified post hoc after selecting sets of genes of interest, thus biasing the interpretation of underlying gene regulatory networks.

In this study, we aimed at disentangling miRNA-driven post-transcriptional signals using the pig as a model. We performed an exon-intron split analysis (EISA) to muscle and fat RNA-seq data from two Duroc pig populations subjected to fasting-feeding conditions and with divergent fatness profiles, respectively. After running EISA analyses, protein-coding mRNA genes with downregulated exonic fractions and high post-transcriptional signals were significantly enriched for binding sites of upregulated DE miRNAs. Moreover, these genes showed an increased expression covariation for the exonic fraction compared to that of the intronic fraction. On the contrary, they did not show enrichment for binding sites of highly expressed and/or downregulated DE miRNAs. Among the set of loci displaying miRNA-driven post-transcriptional regulatory signals, we observed genes related to glucose homeostasis (*DKK2*, *PDK4*, *IL18*, *NR4A3*, *CHRNA1*, *TET2*), cell differentiation (*PBX1*, *BACH2*) or adipocytes metabolism (*LEP*, *ESRRG*, *PTGFR*, *SERPINE2*, *RNF157*, *GPLD1*, *OSBPL10*, *PRSS23*). Our results highlighted mRNA genes showing post-transcriptional signals linked to miRNA-driven downregulation by using exonic and intronic fractions of RNA-seq datasets from muscle and adipose tissues in pigs.

Keywords:

Exon-intron split analysis, microRNA, pigs, energy homeostasis.

1. Introduction

RNA dynamics in the cell metabolism are subjected to complex yet poorly characterized regulatory mechanisms that contribute to shaping fine-tuned biological responses to different stimuli [1]. Cellular metabolic changes are hence a direct manifestation of intricate interactions between expressed transcripts and other regulatory elements that modify their abundance, localization, fate and degradation rate. MicroRNAs (miRNAs) are primarily engaged in post-transcriptional control of gene expression through inhibition of translation and/or destabilization of target mRNAs through poly(A) shortening and subsequent degradation [2]. These short non-coding regulatory RNAs trigger changes in the abundance of targeted transcripts, which can ultimately be modelled as covariation patterns that might help unravel direct or indirect molecular interplays regulating biological pathways.

In order to disentangle regulatory functions driven by miRNAs, researchers typically focus on genes of their interest showing significant changes in mRNA abundance or protein levels that such regulatory effectors might putatively target. This approach, however, introduces *post hoc* selection of deregulated genes and *ad hoc* search of predicted interactions between the 3'-UTRs of mRNAs and the seed regions of miRNAs, causing a bias that may obscure other minor but relevant regulatory interactions [2–4].

Several studies have addressed the effects of post-transcriptionally perturbed genes in expression datasets [5–7], or how transcriptional dynamics can reflect the cellular transition between homeostasis and stress-induced responses or differentiation stages [8–11]. In an attempt to capture both regulatory components based on expression data, Gaidatzis *et al.* [5] described the use of intronic mapping sequences as direct indicators of primary mRNA oscillations related to transcriptional activation. This study was

based on early reports describing intronic expression as a proxy of nascent transcription and co-transcriptional splicing events [12–14]. Besides, the post-transcriptional effect was defined as a function of the expressed exonic and intronic fraction [5]. Although many studies have took advantage of this approach to discern transcriptional and post-transcriptional responses within co-expressed mRNAs and their corresponding putative regulators [5–7], its application remains limited.

In the present study, we aimed to characterize miRNA-driven post-transcriptional signals in skeletal muscle in response to nutrient boost after food intake. We also explored post-transcriptional regulatory signals in adipose tissue using an independent pig population with divergent fatness profiles and qPCR analyses for cross-validation. Using a set of expression data from RNA-seq and miRNA-seq experiments, we predicted in silico miRNA-mRNA interactions and we then evaluated the perturbed expression status of relevant genes at the post-transcriptional level beyond canonical differential expression analyses. In this way, we were able to disentangle hidden regulatory effects driven by miRNA post-transcriptional regulation contributing to modulating energy usage, glucose homeostasis and lipids metabolism in the skeletal muscle and adipose tissue of pigs.

2. Materials and methods

2.1. Experimental design and tissue collection

Expression data and experimental conditions employed to infer gene covariation networks and regulatory connections were previously described in [15–17]. In brief, two independent experimental designs comprising expression profiles from mRNAs and miRNAs in Duroc pigs were used:

(i) The transcriptomic profile of *gluteus medius* (GM) skeletal muscle samples from a total of 23 Duroc gilts were measured employing RNA-seq and small RNA-seq sequencing using the same biological material as reported in [15,17,18]. All gilts were fed *ad libitum* during their productive lives [15,18] until reaching ~150 days of age and they were subsequently slaughtered at the IRTA Experimental Slaughterhouse in Monells (Girona, Spain) following Spanish welfare regulations. Prior to slaughtering, all animals were fasted during 12 h. Gilts were then divided in two fasting/feeding regimes, *i. e.* 11 gilts (*AL-T0*) were slaughtered in fasting conditions upon arrival at the abattoir, whereas the rest of the animals were slaughtered immediately after 7 h (*AL-T2*, N =12) with access to *ad libitum* feed intake. After slaughtering, *gluteus medius* skeletal muscle samples were collected, conserved in RNAlater solution (Thermo Fisher Scientific, Barcelona, Spain) and subsequently snap-frozen in liquid nitrogen.

(ii) A total of 10 Duroc-Göttingen minipig inter-cross F2 animals with divergent fatness profiles according to body mass index (BMI) metric (5 *lean* and 5 *obese*) were selected from the UNIK resource population comprising a total of 502 F2 pigs [19,20], as described in Jacobsen et al. 2019 [16]. Pigs were slaughtered when they reach 8-13 months of age according to the Danish "Animal Maintenance Act" (Act 432 dated 09/06/2004). Tissue samples from retroperitoneal tissue of each animal were collected and mature adipocytes were isolated following the protocol of Decaunes et al. 2011 [21] with modifications as reported by Jacobsen et al. 2019 [16]. Once extracted, adipocyte pellets were snap-frozen at -80°C until further experimental procedures.

2.2. RNA extraction and sequencing

RNA extraction, RNA-Seq and small RNA-Seq sequencing protocols, quality-check preprocessing and mapping were performed as previously described [15–17]. In brief,

126 total RNA was isolated from GM tissue using the RiboPure kit (Ambion, Austin, TX),
127 while for RNA from adipocytes, the protocol from Cirera et al. 2013 [22] specifically
128 adapted to adipose tissue was implemented. Sequencing libraries were prepared with
129 dedicated TruSeq stranded total RNA kits (Illumina Inc. CA) [16,17] and paired-end
130 sequenced in a HiSeq 2000 equipment (Illumina Inc. CA). Small RNA-specific libraries
131 were prepared from total RNA isolates following the TruSeq Small RNA Sample
132 Preparation Kit (Illumina Inc., CA) and subjected to single-end (1 x 50 bp) sequencing
133 in a HiSeq 2500 equipment (Illumina Inc., CA).
134
135 **2.3. Quality check, filtering and mapping of sequences**
136 Sequenced reads from RNA-Seq and small RNA-Seq data sets belonging to both fasting
137 and fed Duroc gilts, as well as to lean and obese Duroc-Göttingen minipigs, were
138 trimmed to remove any remaining sequencing adapters and quality-checked with the
139 Cutadapt software [23]. Subsequently, reads were mapped against the Sscrofa11.1
140 porcine reference assembly with the HISAT2 aligner [24] and default parameters for
141 RNA-Seq reads, and with the Bowtie Alignment v.1.2.1.1 software [25] using small
142 sequence reads specifications (*bowtie -n 0 -l 25 -m 20 -k 1 --best --strata*) for small
143 RNA-Seq reads, respectively.
144
145 **2.4. Exon/Intron quantification**
146 We generated exonic and intronic ranges spanning all gene annotations available using
147 the gtf formatted Sscrofa.11.1 v.103 gene annotation file retrieved from Ensembl
148 repositories (http://ftp.ensembl.org/pub/release-103/gtf/sus_scrofa/). Overlapping
149 intronic/exonic regions, as well as singleton positions were removed from intronic
150 ranges [26]. To avoid the counting of exonic reads mapping close to exon/intron

151 junctions that could bias the quantification of intronic regions, we removed 10 basepairs
152 (bp) from both sides of each intronic range.
153 Once the corresponding exonic and intronic ranges for Sscrofa11.1 v.103 were retrieved,
154 we used the featureCounts function within the Rsubread package [27] to quantify gene
155 expression profiles based on exon/intron expression patterns for each gene. MiRNA
156 expression profiles were extracted from small RNA-Seq sequencing data using the
157 Sscrofa11.1 v.103 mature miRNA annotation with featureCounts software tool [28] in
158 single-end mode and with default parameters.
159

160 **2.5. Exon/intron split analysis (EISA) for assessing post-transcriptional effects on**
161 **gene expression**

162 We applied EISA analyses to differentiate gene expression regulation based on post-
163 transcriptional effects [5–7]. To this end, we separately estimated the exonic/intronic
164 abundance of each annotated mRNA gene using the Sscrofa11.1 v.103 exon/intron
165 custom annotation ranges previously generated. Only genes showing average expression
166 values above 1 count-per-million (CPM) in at least 50% of animals were retained for
167 further analyses.
168 Counts were processed following the methods described in Gaidatzis *et al*. [5].
169 Normalization was performed independently for exon and intron counts by multiplying
170 each i^{th} gene expression in each j^{th} sample by the corresponding mean gene expression
171 and dividing by the total number of quantified counts per sample.
172 Normalized and expression filtered gene abundances for exonic and intronic ranges
173 were subsequently transformed in the $\log_2$ scale, adding a pseudo-count of 1.
174 Exon/intron $\log_2$ transformed abundances for each gene were averaged within each

considered treatment groups (*AL-T0* and *AL-T2* for GM tissues and *lean* and *obese* for adipocyte isolates).

Only genes with successful exonic and intronic quantified read counts were further considered in our analyses, hence removing mono-exonic genes and poliexonic genes where exonic and/or intronic expression was undetected. The transcriptional component (Tc) contribution to observed differences in each i^{th} gene expression levels between contrast groups was expressed as the increment of intron counts in fed (*AL-T2*) and *obese* animals with respect to fasting (*AL-T0*) and *lean* animals, respectively, denoted as $\Delta Int = Int_{2i} - Int_{1i}$. The increment of exonic counts ΔEx was defined accordingly, and the post-transcriptional component (PTc) effect was expressed as $\Delta Ex - \Delta Int = (Ex_{2i} - Ex_{1i}) - (Int_{2i} - Int_{1i})$. Both components were z-scored to represent comparable ranges between ΔEx and ΔInt estimates. Post-transcriptional expected effects according to ΔEx and PTc ($\Delta Ex - \Delta Int$) distribution are depicted in **Fig. S1A**. The classification and interpretation of the combinatorial possibilities among ΔEx, ΔInt (Tc) and $\Delta Ex - \Delta Int$ (PTc) values explored in the current work are shown in **Fig. S1B.** All implemented analyses have been summarized in **Fig. S1C**. A ready-to-use modular pipeline for running EISA is publicly available at https://github.com/emarmolsanchez/EISACompR.

2.6. Post-transcriptional signal prioritization

In order to obtain a prioritized list of genes showing meaningful signals of post-transcriptional regulatory activity, the top 5% genes with the highest negative PTc scores were retrieved for each of the two experimental contrasts (i.e., *AL-T0* vs *AL-T2* from Duroc GM muscle and *lean* vs *obese* from UNIK Duroc-Göttingen adipocytes). We only focused on genes showing strong reduced ΔEx values > 2 folds for post-transcriptional signals in *AL-T0* vs *AL-T2* animals and reduced ΔEx > 3 folds in *lean* vs

obese animals. The higher fold change in exonic fractions used for the *lean* vs *obese* experimental design was motivated by the overall weaker differential expression obtained at both mRNA and miRNA levels for these data sets. MiRNAs actin as post-transcriptional repressors of targeted mRNAs were considered as the main effectors of the observed mRNA downregulation.

2.7. Differential expression and significance of regulatory signals

Canonical differential expression analyses were carried out with the *edgeR* package [29] using the exonic fraction of mRNAs and miRNA expression profiles from RNA-Seq and small RNA-Seq data sets comprising *AL-T0 vs AL-T2* and *lean vs obese contrasts*. Expression filtered raw counts for exonic reads were normalized with the trimmed mean of M-values normalization (TMM) method [30]. Subsequently, after dispersion estimation with a Cox-Reid profile-adjusted likelihood method [31], a generalized log-linear model of the negative binomial distribution was fitted and significance in expression differences was tested with a quasi-likelihood F-test implemented in the glmQLFit function from edgeR method [29]. Correction for multiple hypothesis testing was applied using the Benjamini-Hochberg false discovery rate approach [32]. Genes were considered as differentially expressed (DE) when they had $|FC| > 2$ and q-value < 0.05 for mRNAs, and $|FC| > 1.5$ and q-value < 0.05 for miRNAs.

The statistical significance of the post-transcriptional (PTc) component variation between groups (*AL-T0 vs AL-T2* and *lean vs obese*) was evaluated using *edgeR* and incorporating the intronic quantification as an interaction factor for exonic abundances. In this way we accounted for the previous intronic variation effect on the differences shown at the exonic level for the mature mRNA after intron splicing.

2.8. miRNA target prediction

Target interactions between the seed regions of expressed miRNAs from small RNA-seq datasets and 3'-UTRs of expressed protein-coding mRNA genes from RNA-seq datasets were assessed on the basis of sequence identity using the Sscrofa11.1 reference assembly. The annotated 3'-UTRs from porcine mRNAs were retrieved from Sscrofa11.1 v.103 available at bioMart database (http://www.ensembl.org/biomart) and miRBase database [33]. The 3'-UTR sequences shorter than 30 nts were discarded. Redundant seeds from mature porcine microRNAs were removed.

The seedVicious v1.1 tool [34] was used to infer miRNA-mRNA interactions against the non-redundant set of porcine miRNA seeds and 3'-UTRs retrieved from the Sscrofa11.1 v.103 annotation (http://ftp.ensembl.org/pub/release-103/gtf/sus_scrofa/). MiRNA-mRNA interactions of type 8mer, 7mer-m8 and 7mer-A1 were considered as the most relevant and potentially functional among the set of other alternative non-canonical occurring interactions [2,35,36]. Following early reports about the effects of miRNA binding site context in determining the miRNA-mRNA interaction efficacy [35], we removed *in silico*-predicted miRNA-mRNA interactions complying with any of the following criteria: (i) Binding sites are located in 3'-UTRs at less than 15 nts close to the end of the ORF (and the stop codon) or less than 15 nts close to the terminal poly(A) tail, (ii) binding sites are located in the middle of the 3'-UTR in a range comprising 45-55% of the central body of the non-coding sequence and (iii) binding sites lack AU-rich elements in their immediate upstream and downstream flanking regions comprising 30 nts each.

Covariation patterns between miRNAs and their predicted mRNA targets at gene-wise level were assessed on the basis of Spearman´s correlation coefficients (ρ) using the TMM normalized and $\log_2$ transformed expression profiles of the exonic fractions of

mRNA and miRNA genes. Only miRNA-mRNA predicted pairs comprising DE upregulated miRNAs (FC > 1.5; *q*-value < 0.05) and mRNA genes with relevant PTc scores (see post-transcriptional signal prioritization section) were taken into consideration. Correlations were considered significant at *P*-value < 0.05.

2.9. Gene-wise miRNA enrichment analyses

After the identification of mRNA genes showing marked post-transcriptional signals in both experimental conditions considered and the prediction of putative miRNA binding sites in their 3'-UTRs, we sought to determine if the overall number of mRNA genes (gene-wise) targeted by at least one of the upregulated miRNAs (FC > 1.5; *q*-value < 0.05) was significantly enriched. The whole sets of expressed mRNA genes with available 3'-UTRs from both *AL-T0* vs *AL-T2* and *lean* vs *obese* datasets were used as a contrast background for statistical significance of enrichment analyses, which were carried out using the Fisher's exact test implementation included in the *fisher.test* R function. Results were considered significant at *P*-value < 0.05.

Besides, we also tested whether these genes were enriched for binding sites of the top 5% most highly expressed miRNA genes, excluding the significantly upregulated DE miRNAs, as well as for binding sites of significantly downregulated miRNAs (FC < -1.5; *q*-value < 0.05). Upregulated or downregulated miRNAs showing redundant seeds were considered as one single binding site event. Given the relatively low significant differences in miRNA expression obtained for the small RNA-Seq profiles of UNIK Duroc-Gottingen minipigs (*lean* vs *obese*), miRNAs were considered upregulated at FC >1.5 and *P*-value < 0.01 for such experimental setup.

As a control test, we implemented a randomized bootstrap corrected iteration to generate 100 random sets of 10 expressed mature miRNA genes without seed

redundancy. These sets of miRNAs were used as input for miRNA target prediction with the sets of prioritized mRNA genes with the top 5% PTc scores as previously described. The distribution of odds ratios obtained after iterating over each random set of miRNAs (N = 100) were then compared with odds ratios obtained with the set of significantly upregulated miRNAs (FC > 1.5; *q*-value < 0.05).

The *P*-value for the significance of the deviation of observed odds ratios against the bootstrapped odds ratios distribution was defined as, $P - value = 1 - \frac{r+1}{k+1}$, where r is the number of permuted odds ratios with values equal or higher than the observed odds ratio for enrichment analyses with the set of upregulated miRNAs, and k is the number of defined permutations (N = 100).

2.10. Gene covariation network and covariation enrichment score

We hypothesized that genes showing relevant post-transcriptional downregulatory effects might be regulated by the same set of significantly upregulated miRNAs, which could induce shared covariation in their expression profiles at the exonic level. On the contrary, their intronic fractions would be mainly unaffected, as introns would have been excised prior to any given miRNA-driven downregulation, if occurring. In this way, an increased gene covariation might be detectable within the sets of commonly targeted mRNA genes with relevant post-transcriptional signals at the exon but not at the intron level, as opposed to covariation events of these set of genes with the rest of DE genes.

In order to test such hypothesis, we computed pairwise correlation coefficients among the whole set of DE mRNA genes in the *AL-T0* vs *AL-T2* (*q*-value < 0.05, N = 454) and *lean* vs *obese* (*q*-value < 0.05, N = 299) experimental contrasts, with respect to the set of genes with relevant post-transcriptional signals and putatively targeted by DE

upregulated miRNAs. Normalized exonic and intronic estimates in the $\log_2$ scale obtained from EISA analyses were used to compute Spearman's correlation coefficients (ρ) for each possible pair of DE mRNA genes plus those with post-transcriptional signals but not DE (q-value > 0.05), excluding self-correlation pairs. Significant covariation events were identified with the Partial Correlation with Information Theory (PCIT) network inference algorithm [37] implemented in the *pcit* R package [38]. Non-significant covarying pairs were set to zero, while significant covarying pairs with both positive or negative coefficients $|\rho| > 0.6$ where assigned a value of 1.

The functional regulatory implications of miRNAs in shaping covariation patterns were then assessed by a covariation enrichment score (CES) following Tarbier et al. 2020 [39]. Significant differences among the set of exonic, intronic and control CES values were tested with a non-parametric approach using a Mann-Whitney U non-parametric test [40]. Further details about CES calculation and implementation can be found in **Supplementary Methods File S1**.

2.11. Expression analyses of miRNAs and putative mRNA targets by qPCR

Retroperitoneal adipose tissue (~20 ml) was taken from the abdominal cavity of UNIK intercrossed Duroc-Göttingen minipigs pigs quickly after slaughtering (more details about UNIK minipig population are described elsewhere [19,20]). We then isolated adipocyte cells as described in Jacobsen et al. 2019 [16] and they were used for RNA extraction following the method of Cirera (2013) [22]. Total RNA from adipocytes was subsequently employed for quantitative real-time polymerase chain reaction (qPCR) verification of expression changes. Five mRNAs (*LEP*, *OSBLP10*, *PRSS23*, *RNF157* and *SERPINE2*) among the top 5% with the highest negative PTc values and showing reduced ΔEx higher than 3-fold (equivalent to -1.58 in the $\log_{2\ scale}$) were selected for

expression profiling. The same 5 *lean* and 5 *obese* animals (according to BMI profiles, **Table S1**) used for RNA-Seq and small RNA-seq analyses [16,41] were selected, with the exception of animal 572, for which no additional RNA was available and that was replaced by animal 503, which had the closest BMI profile within the *obese* group of animals (**Table S1**). Two reference genes (*TBP* and *ACTB*, according to Nygard et al. 2007 [42]) were used as normalizers. Primers were collected from available stocks from previous studies [42,43] or designed using the PRIMER3 software within the PRIMER-BLAST tool [44], considering exon–exon junction spanning primers for poly-exonic candidates and accounting for multiple transcript capture when possible.

Accordingly, three miRNAs among the most significantly differentially expressed in small RNA sequencing data from UNIK samples were selected for qPCR profiling (ssc-miR-92b-3p, ssc-miR-148a-3p and ssc-miR-214-3p), plus two miRNAs for normalization which were among the most highly expressed and with no differential expression signal in the *lean* vs *obese* small RNA-Seq data set (ssc-let-7a and ssc-miR-23a-3p). The same RNA samples used for mRNA profiling were subsequently processed for microRNA profiling using 50 ng of total RNA for cDNA synthesis in duplicate and following the protocol for microRNAs of Balcells et al. 2011 [45] with recommendations reported by Cirera & Busk 2014 [46]. Primers for miRNA qPCR amplification were designed using the miRprimer software [47]. Further details about qPCR experimental procedures are available in **Supplementary Methods File S1**. All primers for mRNA and miRNA expression profiling are available at **Table S2.** Raw Cq values for each assay are available at **Table S3**.

3. Results

3.1. Determining post-transcriptional signals in porcine skeletal muscle using the EISA approach

After the processing, mapping and quantification of mRNA and miRNA gene expression profiles in GM skeletal muscle samples encompassing 11 fasting (*AL-T0*) and 12 fed (*AL-T2*) Duroc gilts, an average of 45.2 million reads per sample (~93%) were successfully mapped to annotated genes (N = 31,908, including protein coding and non-coding genes) in the Sscrofa11.1 v.103 assembly. Besides, around 2.2 million reads per sample (~42%) from an average of 6.2 million small RNA sequences mapped to annotated porcine miRNA genes (N = 370).

A total of 30,322 genes based on exonic regions and 22,769 genes based on intronic regions were successfully quantified after splitting the reference Sscrofa11.1 v.103 assembly between exonic and intronic ranges. The reduced number of genes for intronic ranges was produced upon the removal of singleton regions, mono-exonic genes and exon-overlapping intronic ranges that could disturb the accurate determination of intronic fractions.

The exonic fraction accounted for an average of 1,923.94 estimated counts per gene, whereas the intronic fraction was represented by an average of 83.02 counts per gene, meaning that counts in exonic ranges exceeded those in intronic ranges by ~23 fold.

EISA analyses were run using exonic and intronic fractions from the *AL-T0* vs *AL-T2* contrast excluding genes with expression levels below 1 CPM in at least 50% of the samples (N = 12). Only genes represented by both exonic and intronic mapping counts were retained, resulting in a total of 9,492 mRNA genes used for determining ΔEx and ΔInt values and using the fasting group (*AL-T0*) as baseline control, i.e., any given upregulation in ΔEx or ΔInt values represents and overexpression in fed (*AL-T2*) over

fasting (*AL-T0*) Duroc gilts. Finally, PTc scores were obtained from z-scored values of ΔEx – ΔInt estimates and differential expression analyses based on exonic fractions were carried out using the 9,492 genes retrieved.

Differential expression analyses resulted in a total of 454 DE genes (q-value < 0.05), and of those, only genes with |FC| > 2 were retained, totaling 52 upregulated and 80 downregulated genes (**Table S4, Fig. S2A**). Besides, differential expression analyses on small RNA-seq data for *AL-T0* vs *AL-T2* pigs revealed a total of 16 DE miRNAs (|FC| > 1.5; q-value < 0.05), of which 8 were upregulated (representing 6 unique miRNA seeds, **Table S5**). The non-redundant seeds of miRNAs with significantly differential upregulation in fed *AL-T2* animals (N = 6; ssc-miR-148a-3p, ssc-miR-7-5p, ssc-miR-30-3p, ssc-miR-151-3p, ssc-miR-374a-3p and ssc-miR-421-5p, **Table S5**) were selected as those potentially affecting genes post-transcriptionally after nutrient supply. Post-transcriptional signal analyses revealed a total of 133 genes with significant post-transcriptional effects (|FC| > 2; q-value < 0.05, **Table S6**), of which three had reduced ΔEx fractions > 2 folds and two of them had significantly negative PTc scores (q-value < 0.05, **Table 1**).

From these results, we aimed at determining relevant genes putatively downregulated by miRNAs at the post-transcriptional level. Genes within the top most extreme 5% negative PTc scores with visibly reduced ΔEx values > 2 folds were selected as genes showing putative miRNA-driven post-transcriptional downregulation (**Fig. S2B**). This resulted in a total of 26 selected genes (**Table 1**), from which one of them did not have a 3´-UTR annotated (ENSSSCG00000049158) and was hence excluded from miRNA seed target prediction at the 3'-UTR level. Among this set of 26 genes with high post-transcriptional signals, 18 of them were also downregulated considering canonical differential expression analyses on their exonic fractions (FC < -2; q-value < 0.05,

Table 1 and **Table S4**), while three additional genes showed suggestive yet not evidently significant downregulation (*P*-value < 0.01, **Table 1** and **Table S4**).

3.2. Context-based pruning of predicted miRNA-mRNA interactions removes spurious unreliable target events

As a first step to determine if genes with highly negative PTc scores and showing a marked reduction in exonic fractions were possibly affected by the repressor activity of upregulated DE miRNAs (**Table S5**), we aimed to investigate the accuracy and reliability of *in silico* predicted miRNA binding sites in their 3'-UTRs (**Table S7**).

We evaluated the presence of enriched binding sites gene-wise over a random background of expressed genes with no context-based removal of predicted binding sites, applying each one of the three established removal criteria independently (see methods), and combining them pairwise and altogether. As depicted in **Fig. S3A** and **S3B**, introducing additional context-based filtering criteria for removing spurious unreliable binding site predictions resulted in an overall increased enrichment of miRNA targeted genes within the top 1% (**Fig. S3A**) and 5% (**Fig. S3B**) negative PTc scores and with reduced ΔEx > 2 folds. This increased enrichment significance was more prevalent for the AU-rich-based criterion, and was slightly improved when adding the other two context-based removal criteria (**Fig. S3A**). These results were, however, less evident for the list of the top 5% genes (**Fig. S3B**), probably due to the reduced stringency of gene prioritization and the inclusion of putative false positive candidate genes that are not targeted by the non-redundant seeds of detected upregulated miRNAs (N = 6, **Table S5**). Nevertheless, still an increased enrichment was detectable for all combined filtering criteria, especially for binding sites of type 7mer-A1, and probably at the expense of the scarcer and more efficient 8mer binding sites.

Supported by the observed increased reliability of retrieved miRNA binding sites and targeted genes after context-based site pruning, we applied the three joint aforementioned criteria for further target enrichment analyses.

3.3. Genes with relevant post-transcriptional signals are enriched for putative miRNA binding sites in their 3'-UTRs.

Target prediction and context-based pruning of miRNA-mRNA interactions for mRNA genes with the top 5% negative PTc scores and a reduction in the exonic fraction (ΔEx) of at least 2 folds (N = 25 after excluding ENSSSCG00000049158) resulted in a total of 11 binding sites of type 8mer, 21 of type 7mer-m8 and 22 of type 7mer-A1 (**Table S7**) belonging to non-redundant seeds of DE upregulated miRNAs (N = 6) in *AL-T2* gilts (**Table S5**).

Furthermore, we aimed at investigating if these genes showing putative post-transcriptional signals were enriched for miRNA-derived target events at the gene-wide level (i.e., assessing whether the number of these genes being putative targets of upregulated miRNAs were significantly higher compared with a random background). The set of genes with the top 5% (N = 25, **Fig. 1A**) PTc scores and reduced ΔEx > 2 folds obtained significant enrichment results (*P*-value < 0.05) for 8mer, 7mer-m8 and 7mer-A1 targeted genes (**Fig. 1B**), and this was especially relevant for all target types combined. More importantly, 21 out of 25 genes from the top 5% PTc scores (**Table S7**) were predicted as putative targets for miRNAs upregulated in *AL-T2* fed gilts (**Table S5**), the majority of which were concentrated among those with the highest PTc scores (**Table 1**). The gene with the highest post-transcriptional signal was the Dickkopf WNT Signaling Pathway Inhibitor 2 (*DKK2*, **Table 1**), and was the only gene gathering two miRNA binding sites of type 8mer simultaneously (**Table S7**). Other genes with the

top PTc score that gathered multiple miRNA binding sites were, to mention a few, pyruvate dehydrogenase kinase 4 (*PDK4*), interleukin 18 (*IL18*), nuclear receptor subfamily 4 group A member 3 (*NR4A3*) or cholinergic receptor nicotinic α1 subunit (*CHRNA1*). The most relevant miRNAs gathering the highest amount of significant miRNA-mRNA interactions in terms of their correlation patterns were ssc-miR-30a-3p and ssc-miR-421-5p, which showed 9 and 8 significant miRNA-mRNA interactions, followed by ssc-miR-148-3p with a total of 4 significant interactions among the set of mRNA genes with post-transcriptional signals (**Table S7**).

A special case was represented by the ENSSSCG00000049158 gene (**Table 1** and **Table S8**), with no 3'-UTR available in the Sscrofa11.1 annotation. Interestingly, this gene has a relatively long and fragmented 5'-UTR, and we decided to investigate whether putative miRNA targets could happen in this region. No context-based filtering was implemented for these analyses. Surprisingly, we found a total of 7 and 9 binding sites (**Table S8**) for the set of DE upregulated miRNAs (**Table S5**) across the two annotated transcripts of this gene, respectively.

We also evaluated the gene-wise enrichment for this set of genes (N = 25, **Table 1**) with the following sets of miRNAs: (i) Non-redundant seeds from downregulated miRNAs in *AL-T2* fed gilts (ssc-miR-1285, ssc-miR-758, ssc-miR-339, sc-miR-22-3p, ssc-miR-296-5p, ssc-miR-129a-3p, ssc-miR-181c and ssc-miR-19b, **Table S5**), (ii) the top 5% most expressed non-redundant miRNA seeds, excluding those being upregulated, if present (ssc-miR-1, ssc-miR-133a-3p, ssc-miR-26a, ssc-miR-10b, ssc-miR-378, ssc-miR-99a-5p, ssc-miR-27b-3p, ssc-miR-30d, ssc-miR-486 and ssc-let-7f-5p) and (iii) for an iteration (N = 100) of random sets of 10 expressed miRNAs, irrespective of their DE and abundance status, as a control test. None of these additional analyses recovered a

474 significant enrichment for any type of the three considered miRNA target subtypes (**Fig.**
475 **1B**).
476 To exclude the possibility that any additional DE downregulated mRNA genes (**Table**
477 **S4**) were also putatively regulated by miRNAs, removing those previously analyzed for
478 post-transcriptional signals (which were not necessarily downregulated in a significant
479 manner), we also repeated our enrichment analyses for binding sites on this set of genes
480 with 3'-UTR available (N = 48). When we analyzed the enrichment of the number of
481 DE downregulated genes (**Fig. 1C**) being putative targets of upregulated, downregulated
482 or highly expressed miRNAs, no significant results were observed, except for a slight
483 enrichment of genes targeted for highly expressed miRNAs considering 8mer + 7mer-
484 m8 binding sites only (**Fig. 1D**).
485
486 **3.4. Studying post-transcriptional signals in adipocytes metabolism using an**
487 **independent Duroc-Göttingen minipig population**
488 We decided to evaluate the performance of EISA analyses on the miRNA target
489 prioritization using an additional independent experimental setup with the adipocyte
490 mRNA and miRNA expression profiles of a Duroc-Göttingen minipig population with
491 divergent fatness profiles well characterized at the metabolic and molecular level
492 [19,20]. A total of 10 animals divided into two groups of 5 animals each with high and
493 low BMI profiles (*lean* vs *obese*, **Table S1**) were selected for sequencing of adipocyte
494 homogenates collected from retroperitoneal adipose tissue. After pre-processing and
495 filtering of sequenced reads, an average of ~98.1 and ~0.87 million mRNA and small
496 RNA reads per sample were generated, of which ~96.5% and ~73.4% mapped to
497 annotated porcine mRNA and miRNA genes, respectively. Differential expression
498 analyses revealed a total of 299 DE mRNAs (q-value < 0.05), of which 52 mRNAs were

499 downregulated and 95 were upregulated (|FC| > 2; *q*-value < 0.05), respectively (**Table**
500 **S9**). Regarding miRNAs, only one gene (ssc-miR-92b-3p) was significantly upregulated
501 in *lean* pigs (|FC| > 2; *q*-value < 0.05), while 7 additional miRNAs showed suggestive
502 differential expression (*P*-value < 0.01, **Table S10**).
503 After running EISA analyses on the mRNA expression profiles for exonic and intronic
504 fractions, a total of 15 downregulated mRNAs in *lean* pigs were among the top 5% PTc
505 scores with reduced ΔEx > 3 folds (**Table 2, Fig. 2A**). The whole set of mRNA genes
506 from PTc EISA analyses is available at **Table S11**. A total of 12 out of the initial 15
507 mRNA genes were then classified as putative miRNA targets from the set of
508 upregulated miRNA genes in *lean* pigs (ssc-miR-92b-3p, ssc-miR-148a-3p, ssc-miR-
509 204 and ssc-miR-214-3p; **Table S10**), respectively. Among these, it is worth
510 mentioning leptin (*LEP*), oxysterol binding protein like 10 (*OSBPL10*), serine protease
511 23 (*PRSS23*), ring finger protein 157 (*RNF157*), serpin family E member 2
512 (SERPINE2), estrogen related receptor γ (*ESRRG*) or prostaglandin F receptor
513 (*PTGFR*). Moreover, the number of obtained miRNA-mRNA interactions were 1 of
514 type 8mer, 10 of type 7mer-m8 and 11 of type 7mer-A1 (**Table S12**). The strongest
515 covariation patterns among miRNAs and targeted mRNAs were those between ssc-miR-
516 204, ssc-miR-214-3p and ssc-miR92b-3p (**Table S12**), which were also the miRNAs
517 showing the more relevant significant differences in overexpression in *lean* pigs (**Table**
518 **S10**).
519 Gene-wise enrichment analyses for the set of putative miRNA target genes with post-
520 transcriptional signals (N = 12, **Table 2** and **Table S12**) revealed a slight yet consistent
521 enrichment for miRNA targets of type 7mer-m8 and 7mer-A1, although it did not reach
522 significant levels (*P*-value > 0.05, **Fig. 2B**). Nonetheless, these binding sites showed
523 suggestive enrichment compared to analyses assessing the presence of enriched miRNA

target genes with the set of downregulated miRNAs in *lean* pigs (ssc-miR-190a and ssc-miR-1839-5p), as well as with those within the top 5% most highly expressed miRNAs (**Table S10**, **Fig. 2B**).

Furthermore, in order to validate the results obtained for mRNAs with high post-transcriptional signals and the miRNAs putatively interacting with them, we selected 5 mRNAs (*LEP*, *OSBPL10*, *PRSS23*, *RNF157* and *SERPINE2*) and 3 miRNAs (ssc-miR-148a-30, ssc-miR-214-3p and ssc-miR-92b-3p) for qPCR expression profiling verification. All the analyzed mRNA genes showed a reduced expression in *lean* pigs compared with their *obese* counterparts (**Fig. 2C**) and the *LEP* gene was the most significantly downregulated gene (*P*-value = 1.12E-10), a result that was in agreement with the strong downregulation observed in differential expression analyses of the RNA-Seq data set (**Table S9**). With regard to miRNAs, the oppositive expression pattern was revealed, with all the three profiled miRNA genes being upregulated in *lean* pigs. Moreover, as described in the small RNA-Seq differential expression results (**Table S10**), the ssc-miR-92b-3p gene was the miRNA with the most significant upregulation observed in qPCR analyses (*P*-value = 3.57E-02, **Fig. 2D**).

3.5. Genes showing post-transcriptional regulatory signals predominantly covary at the exonic level.

To further elucidate whether genes with top 5% post-transcriptional regulatory signals could account for truly targeted genes by miRNAs according to in silico predictions (N = 21), we evaluated the covariation patterns among them and with the whole set of DE mRNA genes (*q*-value < 0.05, N = 454) in our RNA-seq data from *AL-T0* and *AL-T2* gilts. In this way, if a set of genes were to be downregulated by any upregulated miRNAs in a coordinated manner, we would expect a reduced abundance in their

mature spliced mRNA forms, i.e., only the exonic fractions but not the intronic fractions might predominantly covary. The intronic fraction, eventually spliced and degraded in the nucleus, should not reflect any posterior post-transcriptional regulatory effects in the cytoplasm, and a reduced or null covariation in their abundances might be expected.

Using CES values previously described for the top 5% mRNA genes with highest negative PTc scores, reduced ΔEx fractions > 2 folds and putatively targeted by DE upregulated miRNAs (N = 21), we obtained an estimation of the fold change in their observed covariation with respect to other DE mRNAs (N = 435), and this was measured for both their exonic and their intronic abundances. Our analyses revealed that set of mRNA genes with the top 5% negative PTc scores and reduced ΔEx > 2 folds predicted as miRNA targets (N = 21, **Table S7**) of upregulated miRNAs (N = 6, **Table S5**) showed an average significantly increased covariation of ~2 folds in their exonic fractions compared with their intronic fractions (**Fig. 3A**). When we analyzed the observed fold change in covariation for random sets of genes iteratively (N = 1,000), they fell towards null covariation changes, i.e., CES ≈ 1 (**Fig. 3A**). The observed CES distributions of exonic, intronic and control sets were significantly different after running non-parametric tests (**Fig. 3A**), thus supporting the expected predominant effect at the exon level by miRNA-driven post-transcriptional downregulation.

In agreement with results obtained for the *AL-T0* vs *AL-T2* contrast, an increased covariation of ~2 folds was also observed for exonic and intronic fractions of putatively targeted mRNA genes (N = 12) by DE upregulated miRNAs in the *lean* vs *obese* contrast, although not at a significant level (**Fig. 3B**).

Moreover, 19 out of 21 (*AL-T0* vs *AL-T2*) and 9 out of 12 (*lean* vs *obese*) analyzed mRNA genes putatively targeted by DE upregulated miRNAs showed an overall increased covariation in their exonic fractions compared with their intronic fractions,

574 expressed as the increment in their CES values (ΔCES = exonic CES – intronic CES,
575 **Table S13**). From these, the mRNA genes with a highest fold change increment in
576 exonic covariation were, to mention a few, the Dickkopf WNT Signaling Pathway
577 Inhibitor 2 (*DKK2*), which also had the highest post-transcriptional signal (**Table 1**),
578 leucine rich repeat neuronal 1 (*LRRN1*), PBX homeobox 1 (*PBX1*), cholinergic receptor
579 nicotinic α1 subunit (*CHRNA1*), Tet methylcytosine dioxygenase 2 (*TET2*), 6-
580 Phosphofructo-2-Kinase/Fructose-2,6-Biphosphatase 3 (*PFKFB3*) or nuclear receptor
581 subfamily 4 group A member 3 (*NR4A3*) for the *AL-T0* vs *AL-T2* contrast, as well as
582 glycosylphosphatidylinositol specific phospholipase D1 (*GPLD1*), tumor protein P53
583 inducible protein 11 (*TP53I11*), serine protease 23 (*PRSS23*) or estrogen related
584 receptor γ (*ESRRG*) for the *lean* vs *obese* contrast.
585
586

587 # 4. Discussion

588 In the present study we have applied and exon/intron split approach [5], which provides
589 an unbiased methodology to prioritize mRNA genes showing post-transcriptional
590 downregulatory signals linking them to upregulated miRNAs that might be targeting
591 these mRNAs and triggering their observed decay in differential expression analyses.
592 Motivated by the notion that genes showing strong downregulation in exonic variance
593 (ΔEx) between groups, combined with highly negative PTc scores (ΔEx – ΔInt), would
594 represent a proxy for post-transcriptionally regulated genes, we selected those mRNAs
595 showing a reduced exonic fraction while also having highly negative PTc scores. The
596 strong downregulation observed in ΔEx values would exceed that observed in the ΔInt
597 fraction, resulting in a lack of intronic downregulation that might result from post-
598 transcriptional changes only at the exonic level after mRNA splicing in the nucleus.

We observed that the majority of mRNA genes with highly negative PTc scores, i.e., predominantly downregulated at their exonic fractions, also had a coordinated downregulatory effect in their intronic fractions, taken as a proxy of transcriptional repression. This was evidenced by the overall low significance of post-transcriptional signals within the mRNA genes with the top 5% negative PTc scores and reduced ΔEx in both analyzed experimental conditions (**Tables 1** and **2**). It is worth noting that we did not consider the significance of PTc scores as a relevant criterion for prioritizing putative post-transcriptionally downregulated genes, as these will appear as significant only when the post-transcriptional activity was the unique mechanism modulating the target gene expression profile. Only co-occurring yet opposite transcriptional and post-transcriptional events or single post-transcriptional signals would arise as significant, excluding those genes with both coordinated downregulation at the post-transcriptional level. Only two genes (*DKK2* and *NAV2*) in the *AL-T0* vs *AL-T2* contrast showed significant PTc scores (q-value < 0.05, **Table 1**), revealing the overall coordinated downregulatory effect at transcriptional and post-transcriptional level we found, which is in agreement with previous reports using EISA [6,7].

Since the efficacy of miRNA targeting depends on the context of the target site within the 3'-UTR [35], we have described the usefulness of introducing context-based filtering criteria for removing spurious in silico-predicted target sites for miRNAs. The increase in enrichment significance shown for targeted mRNAs with post-transcriptional signals and upregulated miRNAs, as opposed to other highly expressed and/or downregulated miRNAs, highlighted the ability of such criteria to discriminate and remove weak or false positive target sites located within unfavored regions of the 3'-UTR. However, highly efficient target sites such as those of type 8mer, although scarcer than 7mer-m8 sites, might still be functional even at unfavored positions

[35,48,49], which may partially explain the relative lack of 8mer sites found in the top post-transcriptionally regulated mRNA genes.

We opted for using the intronic fraction of expressed mRNAs as a proxy of their transcriptional activity. In this way, the intronic fraction might reflect an approximation to transcriptional activity of yet unspliced mRNA transcripts leading to the accumulation of intronic sequences prior to their debranching and degradation by exonucleases. Previous reports have also explored the use of specific techniques to capture nascent transcripts before they are spliced [8,50,51], and these have been used to account for the transcriptional activity in a similar approach to EISA [52]. The use of intronic fractions as a signal of transcription allows the use of RNA-seq datasets to apply EISA without the need of further experimental procedures and it can also be applied to investigate transcriptional regulatory signals [7]. Nevertheless, the use of more advanced methodologies to measure transient transcription of mRNAs might provide a better resolution for future experimental designs [52], while EISA would be still useful to explore already available RNA-seq data.

From the analysis of top mRNA genes showing the strongest post-transcriptional downregulatory effects in fasted (*AL-T0*) vs fed (*AL-T2*) gilts, relevant biological functions putatively regulated by miRNAs were highlighted. The *DKK2* gene was the one showing the highest negative PTc score, and its post-transcriptional regulatory signal was also significant (**Table 1**), meaning that no additional coordinated transcriptional downregulation was found for this particular gene. Moreover, this gene also showed the strongest covariation difference in its exonic fraction compared with its intronic fraction (**Table S13**). This consistent post-transcriptional regulatory effect might be explained by the presence of two miRNA target sites of type 8mer in its 3´-UTR for ssc-miR-421-5p and ssc-miR-30a-3p, two differentially upregulated miRNAs

649 in the same experimental setup (**Table S5**). Besides, ssc-miR-30e-3p, a miRNA sharing
650 its seed and regulatory effect with ssc-miR-30a-3p, was also upregulated in fed (*AL-T2*)
651 gilts, which would reinforce the repression of the mRNA transcripts. The *DKK2* gene is
652 a member of the dickkopf family that inhibits the Wnt signaling pathway through its
653 interaction with the LDL-receptor related protein 6 (*LRP6*). Its repression has been
654 associated with reduced blood-glucose levels and improved glucose uptake [53], as well
655 as with improved adipogenesis [54] and inhibition of aerobic glycolysis [55]. Moreover,
656 the miR-493-5p, a miRNA that was also upregulated in fed gilts (**Table S5**) although
657 only at nominal level, has been shown to directly regulate its expression [55]. These
658 results would be in agreement with the increased glucose usage and triggered
659 adipogenesis in muscle tissue after nutrient supply. Other additional relevant post-
660 transcriptionally downregulated mRNA genes worth mentioning are: *PDK4*, a
661 mitochondrial enzyme that inhibits pyruvate to acetyl-CoA conversion thus hindering
662 glucose utilization and that promotes fatty acids oxidation in energy-deprived cells
663 under fasting conditions [56,57], *IL18*, a proinflammatory interleukin involved in
664 controlling energy homeostasis in the muscle by inducing AMP-activated protein kinase
665 (AMPK) [58], a master metabolic regulator that is suppressed upon nutrient influx in
666 cells [59], *NR4A3*, an orphan nuclear receptor that activates both glycolytic and
667 glycogenic factors [60], as well as β-oxidation in muscle cells [61], *CHRNA1*, the α
668 subunit of the nicotinic cholinergic receptor of muscle cells, whose repression was
669 linked to the inhibition of nicotine-dependent *STAT3* upregulation [62], a transcription
670 factor that promotes insulin resistance in muscle [63], *PBX1*, a stage-specific regulator
671 of adipocyte differentiation [64], *TET2*, a tumor suppressor linked to glucose-dependent
672 AMPK phosphorylation [65] and BTB domain and CNC homolog (*BACH2*), whose
673 inhibition is directly associated with mTOR complex 2 (mTORC2) glucose-dependent

674 activation [66,67] and the repression of forkhead box protein O1 (*FOXO1*) [68] and
675 *PDK4* in a coordinated manner [17,69]. Overall, the highlighted downregulated genes in
676 the muscle of fed gilts after nutrient supply pointed towards a common regulatory
677 function of miRNAs in modulating glucose uptake and energy homeostasis of the
678 skeletal myocytes.

679 Although miRNAs were the major post-transcriptional regulators that we considered in
680 this study, it is important to remark that other additional post-transcriptional
681 modifications and interactions might be responsible of the observed downregulation of
682 mRNAs [70–74]. This could explain the presence of non-miRNA targets within the top
683 post-transcriptional signals, as well as additional regulatory mechanisms not directly
684 involved in energy homeostasis or glucose usage among the highlighted genes. For
685 instance, three circadian clock-related mRNA genes that showed high post-
686 transcriptional signals were the circadian associated repressor of transcription (*CIART*),
687 period 1 (*PER1*) and salt inducible kinase 1 (*SIK1*), yet the first two were not detected
688 as targets of differentially expressed miRNAs, as shown in **Table 1**. As previously
689 reported for this experimental design [15], the presence of several genes showing
690 abundance differences might reflect a tight feedback interplay among them, where their
691 expression and accumulation are coordinately regulated.

692 Regarding EISA analyses in RNA-seq profiles of adipocytes from lean and obese
693 Duroc-Göttingen minipigs, several of the mRNA genes that showed high post-
694 transcriptional repression were involved in lipids metabolism and the regulation of
695 energy homeostasis. For instance, the gene showing the highest post-transcriptional
696 signal was *ESRRG*, an orphan nuclear receptor that modulates oxidative metabolism and
697 mitochondrial function in adipose tissue and that results in the downregulation of
698 adipogenic markers and adipocyte differentiation when repressed [75]. The

prostaglandin F2- receptor protein (PTGFR) overexpression has been associated with hypertension and obesity-related risks [76], and its repression improved insulin sensitivity and glucose homeostasis [77]. High expression of *SERPINE2* gene and its paralog *SERPINE1* were linked to obesogenic states and diabetic symptoms [78], while their inhibition improved glucose metabolism [79]. The serine protease PRSS23 regulates insulin sensitivity and cytokine expression in adipose tissue, and its downregulation confers protective effects against inflammation, reduced fasting glucose level and improved insulin resistance [80], while a high expression of *RNF157* has been described in adipose tissue with high fatness profiles and increased autophagy [81]. Silencing of ORP10 protein, encoded by the *OSBLP10* gene, promotes low-density lipoprotein (LDL) synthesis and inhibits lipogenesis [82]. The serum levels of GPLD1, the gene showing the highest increase in covariation at the exonic fraction (**Table S13**), are regulated by insulin and glucose metabolism [83] and linked to the development of insulin resistance and metabolic syndrome [84]. Finally, leptin production was also decreased in lean pigs compared to their obese counterparts, and was among the top post-transcriptionally regulated mRNA genes. This adipokine is mainly produced in adipose tissue [85] and regulates appetite, energy expenditure and body weight [86,87].

In summary, similar to what we found for glucose metabolism and energy homeostasis in fasted vs fed Duroc pigs, we were also able to describe a set of post-transcriptionally regulated genes in lean vs obese minipigs related to adipose tissue metabolism regulation dependent of their fatness profiles.

5. Conclusions

In this study we have implemented an exon/intron split analysis of RNA-seq data from skeletal muscle and adipose tissue of pigs, in order to disentangle miRNA-driven post-transcriptional signals that are not evident from the solely analysis of differentially expressed mRNAs comparing divergent experimental conditions. In this way, we were able to prioritize regulatory relationships between upregulated miRNAs and their putative mRNA targets. We demonstrated that incorporating context-based pruning of in silico-predicted miRNA targets increased the reliability of the putative miRNA-mRNA interactions. Besides, these downregulated mRNAs with relevant post-transcriptional signals were significantly enriched for being cooperatively targeted by a set of upregulated miRNAs, as opposed to other highly expressed and/or downregulated miRNAs. The majority of these genes showed an average of 2-folds increase in expression covariation in their exonic fractions compared to their intronic fractions, a result that reinforced their putative post-transcriptional downregulation by miRNA-driven transcript decay. Our results highlight an efficient framework to prioritize mRNA genes showing post-transcriptional signals linked to miRNA-driven downregulation using exonic and intronic fractions of commonly available RNA-seq datasets.

Support

The present research work was funded by grants AGL2013-48742-C2-1-R and AGL2013-48742-C2-2-R awarded by the Spanish Ministry of Economy and Competitivity. E. Mármol-Sánchez was funded with a PhD fellowship FPU15/01733 awarded by the Spanish Ministry of Education and Culture (MECD).

Conflict of interest

The authors declare no conflict of interest.

Acknowledgements

The authors would like to thank the Department of Veterinary Animal Sciences in the Faculty of Health and Medical Sciences of the University of Copenhagen for providing sequencing data and their facilities and resources for RT-qPCR experiments. We also acknowledge Selección Batallé S.A. for providing animal material and the Spanish Ministry of Economy and Competitivity for the Center of Excellence Severo Ochoa 2016-2019 (SEV-2015-0533) grant awarded to the Center for Research in Agricultural Genomics (CRAG). Thanks also to the CERCA Programme of the Generalitat the Catalunya for their support.

References

[1] N.J. Martinez, A.J.M. Walhout, The interplay between transcription factors and microRNAs in genome-scale regulatory networks, BioEssays. 31 (2009) 435–445. doi:10.1002/bies.200800212.

[2] D.P. Bartel, Metazoan microRNAs, Cell. 173 (2018) 20–51.doi:10.1016/j.cell.2018.03.006.

[3] D. Baek, J. Villén, C. Shin, F.D. Camargo, S.P. Gygi, D.P. Bartel, The impact of microRNAs on protein output, Nature. 455 (2008) 64–71. doi:10.1038/nature07242.

[4] M.S. Ebert, P.A. Sharp, Roles for microRNAs in conferring robustness to biological processes, Cell. 149 (2012) 515–524. doi:10.1016/j.cell.2012.04.005.

774 [5] D. Gaidatzis, L. Burger, M. Florescu, M.B. Stadler, Analysis of intronic and
775 exonic reads in RNA-seq data characterizes transcriptional and post-
776 transcriptional regulation, Nat. Biotechnol. 33 (2015) 722–729.
777 doi:10.1038/nbt.3269.
778 [6] J. Cursons, K.A. Pillman, K.G. Scheer, P.A. Gregory, M. Foroutan, S. Hediyeh-
779 Zadeh, J. Toubia, E.J. Crampin, G.J. Goodall, C.P. Bracken, M.J. Davis,
780 Combinatorial targeting by microRNAs co-ordinates post-transcriptional control
781 of EMT, Cell Syst. 7 (2018) 77-91.e7. doi:10.1016/j.cels.2018.05.019.
782 [7] K.A. Pillman, K.G. Scheer, E. Hackett-Jones, K. Saunders, A.G. Bert, J. Toubia,
783 H.J. Whitfield, S. Sapkota, L. Sourdin, H. Pham, T.D. Le, J. Cursons, M.J. Davis,
784 P.A. Gregory, G.J. Goodall, C.P. Bracken, Extensive transcriptional responses
785 are co-ordinated by microRNAs as revealed by Exon–Intron Split Analysis
786 (EISA), Nucleic Acids Res. 47 (2019) 8606-8619. doi:10.1093/nar/gkz664.
787 [8] L.J. Core, J.J. Waterfall, J.T. Lis, Nascent RNA sequencing reveals widespread
788 pausing and divergent initiation at human promoters, Science. 322 (2008) 1845–
789 1848. doi:10.1126/science.1162228.
790 [9] Y.L. Khodor, J. Rodriguez, K.C. Abruzzi, C.-H.A. Tang, M.T. Marr, M.
791 Rosbash, Nascent-seq indicates widespread cotranscriptional pre-mRNA splicing
792 in Drosophila., Genes Dev. 25 (2011) 2502–12. doi:10.1101/gad.178962.111.
793 [10] A. Zeisel, W.J. Köstler, N. Molotski, J.M. Tsai, R. Krauthgamer, J. Jacob-Hirsch,
794 G. Rechavi, Y. Soen, S. Jung, Y. Yarden, E. Domany, Coupled pre-mRNA and
795 mRNA dynamics unveil operational strategies underlying transcriptional
796 responses to stimuli., Mol. Syst. Biol. 7 (2011) 529. doi:10.1038/msb.2011.62.
797 [11] G. La Manno, R. Soldatov, A. Zeisel, E. Braun, H. Hochgerner, V. Petukhov, K.
798 Lidschreiber, M.E. Kastriti, P. Lönnerberg, A. Furlan, J. Fan, L.E. Borm, Z. Liu,

D. van Bruggen, J. Guo, X. He, R. Barker, E. Sundström, G. Castelo-Branco, P. Cramer, I. Adameyko, S. Linnarsson, P. V Kharchenko, RNA velocity of single cells., Nature. 560 (2018) 494–498. doi:10.1038/s41586-018-0414-6.

[12] A. Ameur, A. Zaghlool, J. Halvardson, A. Wetterbom, U. Gyllensten, L. Cavelier, L. Feuk, Total RNA sequencing reveals nascent transcription and widespread co-transcriptional splicing in the human brain., Nat. Struct. Mol. Biol. 18 (2011) 1435–40. doi:10.1038/nsmb.2143.

[13] J.M. Gray, D.A. Harmin, S.A. Boswell, N. Cloonan, T.E. Mullen, J.J. Ling, N. Miller, S. Kuersten, Y.-C. Ma, S.A. McCarroll, S.M. Grimmond, M. Springer, SnapShot-Seq: a method for extracting genome-wide, in vivo mRNA dynamics from a single total RNA sample., PLoS One. 9 (2014) e89673. doi:10.1371/journal.pone.0089673.

[14] G.-J. Hendriks, D. Gaidatzis, F. Aeschimann, H. Großhans, Extensive oscillatory gene expression during C. elegans larval development., Mol. Cell. 53 (2014) 380–92. doi:10.1016/j.molcel.2013.12.013.

[15] T.F. Cardoso, R. Quintanilla, J. Tibau, M. Gil, E. Mármol-Sánchez, O. González-Rodríguez, R. González-Prendes, M. Amills, Nutrient supply affects the mRNA expression profile of the porcine skeletal muscle, BMC Genomics. 18 (2017) 603. doi:10.1186/s12864-017-3986-x.

[16] M.J. Jacobsen, J.H. Havgaard, C. Anthon, C.M.J. Mentzel, S. Cirera, P.M. Krogh, S. Pundhir, P. Karlskov-Mortensen, C.S. Bruun, P. Lesnik, M. Guerin, J. Gorodkin, C.B. Jørgensen, M. Fredholm, R. Barrès, Epigenetic and transcriptomic characterization of pure adipocyte fractions from obese pigs identifies candidate pathways controlling metabolism, Front. Genet. 10 (2019) 1268. doi:10.3389/fgene.2019.01268.

824 [17] E. Mármol-Sánchez, Y. Ramayo-Caldas, R. Quintanilla, T.F. Cardoso, R.
825 González-Prendes, J. Tibau, M. Amills, Co-expression network analysis predicts
826 a key role of microRNAs in the adaptation of the porcine skeletal muscle to
827 nutrient supply, J. Anim. Sci. Biotechnol. 11 (2020) 10. doi:10.1186/s40104-019-
828 0412-z.
829 [18] M. Ballester, M. Amills, O. González-Rodríguez, T.F. Cardoso, M. Pascual, R.
830 González-Prendes, N. Panella-Riera, I. Díaz, J. Tibau, R. Quintanilla, Role of
831 AMPK signalling pathway during compensatory growth in pigs, BMC Genomics.
832 19 (2018) 682. doi:10.1186/s12864-018-5071-5.
833 [19] L.J.A. Kogelman, H.N. Kadarmideen, T. Mark, P. Karlskov-Mortensen, C.S.
834 Bruun, S. Cirera, M.J. Jacobsen, C.B. Jørgensen, M. Fredholm, An F2 pig
835 resource population as a model for genetic studies of obesity and obesity-related
836 diseases in humans: Design and genetic parameters, Front. Genet. 4 (2013) 29.
837 doi:10.3389/fgene.2013.00029.
838 [20] S.D. Pant, P. Karlskov-Mortensen, M.J. Jacobsen, S. Cirera, L.J.A. Kogelman,
839 C.S. Bruun, T. Mark, C.B. Jørgensen, N. Grarup, E.V.R. Appel, E.A.A.
840 Galjatovic, T. Hansen, O. Pedersen, M. Guerin, T. Huby, P. Lesnik, T.H.E.
841 Meuwissen, H.N. Kadarmideen, M. Fredholm, Comparative analyses of QTLs
842 influencing obesity and metabolic phenotypes in pigs and humans, PLoS One. 10
843 (2015) e0137356. doi:10.1371/journal.pone.0137356.
844 [21] P. Decaunes, D. Estève, A. Zakaroff-Girard, C. Sengenès, J. Galitzky, A.
845 Bouloumié, Adipose-derived stromal cells: cytokine expression and immune cell
846 contaminants., Methods Mol. Biol. 702 (2011) 151–161. doi:10.1007/978-1-
847 61737-960-4_12.
848 [22] S. Cirera, Highly efficient method for isolation of total RNA from adipose

849 tissue., BMC Res. Notes. 6 (2013) 472. doi:10.1186/1756-0500-6-472.

850 [23] M. Martin, Cutadapt removes adapter sequences from high-throughput
851 sequencing reads, EMBnet.Journal. 17 (2011) 10. doi:10.14806/ej.17.1.200.

852 [24] D. Kim, B. Langmead, S.L. Salzberg, HISAT: a fast spliced aligner with low
853 memory requirements, Nat. Methods. 12 (2015) 357–360.
854 doi:10.1038/nmeth.3317.

855 [25] B. Langmead, C. Trapnell, M. Pop, S.L. Salzberg, Ultrafast and memory-efficient
856 alignment of short DNA sequences to the human genome, Genome Biol. 10
857 (2009) R25. doi:10.1186/gb-2009-10-3-r25.

858 [26] M. Lawrence, W. Huber, H. Pagès, P. Aboyoun, M. Carlson, R. Gentleman, M.T.
859 Morgan, V.J. Carey, Software for computing and annotating genomic ranges,
860 PLoS Comput. Biol. 9 (2013) e1003118. doi:10.1371/journal.pcbi.1003118.

861 [27] Y. Liao, G.K. Smyth, W. Shi, The R package Rsubread is easier, faster, cheaper
862 and better for alignment and quantification of RNA sequencing reads, Nucleic
863 Acids Res. 47 (2019) e47–e47. doi:10.1093/nar/gkz114.

864 [28] Y. Liao, G.K. Smyth, W. Shi, featureCounts: an efficient general purpose
865 program for assigning sequence reads to genomic features, Bioinformatics. 30
866 (2014) 923–930. doi:10.1093/bioinformatics/btt656.

867 [29] M.D. Robinson, D.J. McCarthy, G.K. Smyth, edgeR: a Bioconductor package for
868 differential expression analysis of digital gene expression data., Bioinformatics.
869 26 (2010) 139–40. doi:10.1093/bioinformatics/btp616.

870 [30] M.D. Robinson, A. Oshlack, A scaling normalization method for differential
871 expression analysis of RNA-seq data, Genome Biol. 11 (2010) R25.
872 doi:10.1186/gb-2010-11-3-r25.

873 [31] D.J. McCarthy, Y. Chen, G.K. Smyth, Differential expression analysis of

multifactor RNA-Seq experiments with respect to biological variation, Nucleic Acids Res. 40 (2012) 4288–4297. doi:10.1093/nar/gks042.

[32] Y. Benjamini, Y. Hochberg, Controlling the false discovery rate: a practical and powerful approach to multiple testing, J. R. Stat. Soc. Ser. B. 57 (1995) 289–300. doi:10.2307/2346101.

[33] A. Kozomara, M. Birgaoanu, S. Griffiths-Jones, MiRBase: From microRNA sequences to function, Nucleic Acids Res. 47 (2019) D155–D162. doi:10.1093/nar/gky1141.

[34] A. Marco, SeedVicious: Analysis of microRNA target and near-target sites, PLoS One. 13 (2018) e0195532. doi:10.1371/journal.pone.0195532.

[35] A. Grimson, K.K.H. Farh, W.K. Johnston, P. Garrett-Engele, L.P. Lim, D.P. Bartel, MicroRNA targeting specificity in mammals: determinants beyond seed pairing, Mol. Cell. 27 (2007) 91–105. doi:10.1016/j.molcel.2007.06.017.

[36] R.C. Friedman, K.K.H. Farh, C.B. Burge, D.P. Bartel, Most mammalian mRNAs are conserved targets of microRNAs, Genome Res. 19 (2009) 92–105. doi:10.1101/gr.082701.108.

[37] A. Reverter, E.K.F. Chan, Combining partial correlation and an information theory approach to the reversed engineering of gene co-expression networks, Bioinformatics. 24 (2008) 2491–2497. doi:10.1093/bioinformatics/btn482.

[38] N.S. Watson-Haigh, H.N. Kadarmideen, A. Reverter, PCIT: an R package for weighted gene co-expression networks based on partial correlation and information theory approaches, Bioinformatics. 26 (2010) 411–413. doi:10.1093/bioinformatics/btp674.

[39] M. Tarbier, S.D. Mackowiak, J. Frade, S. Catuara-Solarz, I. Biryukova, E. Gelali, D.B. Menéndez, L. Zapata, S. Ossowski, M. Bienko, C.J. Gallant, M.R.

899 Friedländer, Nuclear gene proximity and protein interactions shape transcript
900 covariations in mammalian single cells, Nat. Commun. 11 (2020) 5445.
901 doi:10.1038/s41467-020-19011-5.
902 [40] H.B. Mann, D.R. Whitney, On a test of whether one of two random variables is
903 stochastically larger than the other, Ann. Math. Stat. 18 (1947) 50–60.
904 doi:10.1214/aoms/1177730491.
905 [41] P.M. Sørensen, MicroRNA's in obesity and obesity related phenotypes: Using
906 pig as a model, University of Copenhagen, 2014.
907 [42] A.B. Nygard, C.B. Jørgensen, S. Cirera, M. Fredholm, Selection of reference
908 genes for gene expression studies in pig tissues using SYBR green qPCR, BMC
909 Mol. Biol. 8 (2007) 67. doi:10.1186/1471-2199-8-67.
910 [43] C.M.J. Mentzel, F. Alkan, H. Keinicke, M.J. Jacobsen, J. Gorodkin, M.
911 Fredholm, S. Cirera, Joint profiling of miRNAs and mRNAs reveals miRNA
912 mediated gene regulation in the Göttingen minipig obesity model, PLoS One. 11
913 (2016) e0167285. doi:10.1371/journal.pone.0167285.
914 [44] A. Untergasser, I. Cutcutache, T. Koressaar, J. Ye, B.C. Faircloth, M. Remm,
915 S.G. Rozen, Primer3—new capabilities and interfaces, Nucleic Acids Res. 40
916 (2012) e115–e115. doi:10.1093/nar/gks596.
917 [45] I. Balcells, S. Cirera, P.K. Busk, Specific and sensitive quantitative RT-PCR of
918 miRNAs with DNA primers, BMC Biotechnol. 11 (2011) 70. doi:10.1186/1472-
919 6750-11-70.
920 [46] S. Cirera, P.K. Busk, Quantification of miRNAs by a simple and specific qPCR
921 method, in: Methods Mol. Biol. 1182 (2014) 73–81. doi:10.1007/978-1-4939-
922 1062-5_7.
923 [47] P.K. Busk, A tool for design of primers for microRNA-specific quantitative RT-

924 qPCR, BMC Bioinformatics. 15 (2014) 29. doi:10.1186/1471-2105-15-29.

925 [48] R. Denzler, S.E. McGeary, A.C. Title, V. Agarwal, D.P. Bartel, M. Stoffel,
926 Impact of microRNA levels, target-site complementarity, and cooperativity on
927 competing endogenous RNA-regulated gene expression, Mol. Cell. 64 (2016)
928 565-579. doi:10.1016/j.molcel.2016.09.027.

929 [49] S.E. McGeary, K.S. Lin, C.Y. Shi, T.M. Pham, N. Bisaria, G.M. Kelley, D.P.
930 Bartel, The biochemical basis of microRNA targeting efficacy, Science. 366
931 (2019) eaav1741. doi:10.1126/science.aav1741.

932 [50] D.B. Mahat, H. Kwak, G.T. Booth, I.H. Jonkers, C.G. Danko, R.K. Patel, C.T.
933 Waters, K. Munson, L.J. Core, J.T. Lis, Base-pair resolution genome-wide
934 mapping of active RNA polymerasesusing precision nuclear run-on (PRO-seq),
935 Nat. Protoc. 11 (2016) 1455. doi:10.1038/nprot.2016.086.

936 [51] A. Blumberg, Y. Zhao, Y.-F. Huang, N. Dukler, E.J. Rice, A.G. Chivu, K.
937 Krumholz, C.G. Danko, A. Siepel, Characterizing RNA stability genome-wide
938 through combined analysis of PRO-seq and RNA-seq data, BMC Biol. 19 (2021)
939 30. doi:10.1186/s12915-021-00949-x.

940 [52] R.K. Patel, J.D. West, Y. Jiang, E.A. Fogarty, A. Grimson, Robust partitioning of
941 microRNA targets from downstream regulatory changes, Nucleic Acids Res. 48
942 (2020) 9724–9746. doi:10.1093/nar/gkaa687.

943 [53] X. Li, J. Shan, W. Chang, I. Kim, J. Bao, H.-J. Lee, X. Zhang, V.T. Samuel, G.I.
944 Shulman, D. Liu, J.J. Zheng, D. Wu, Chemical and genetic evidence for the
945 involvement of Wnt antagonist Dickkopf2 in regulation of glucose metabolism,
946 Proc. Natl. Acad. Sci. 109 (2012) 11402–11407. doi:10.1073/PNAS.1205015109.

947 [54] J. Yang, B. yin Shi, Dickkopf (Dkk)-2 is a beige fat-enriched adipokine to
948 regulate adipogenesis, Biochem. Biophys. Res. Commun. 548 (2021) 211–216.

949 doi:10.1016/J.BBRC.2021.02.068.

950 [55] F. Deng, R. Zhou, C. Lin, S. Yang, H. Wang, W. Li, K. Zheng, W. Lin, X. Li, X.
951 Yao, M. Pan, L. Zhao, Tumor-secreted dickkopf2 accelerates aerobic glycolysis
952 and promotes angiogenesis in colorectal cancer, Theranostics. 9 (2019) 1001-
953 1014. doi:10.7150/THNO.30056.

954 [56] J.Y. Jeong, N.H. Jeoung, K.-G. Park, I.-K. Lee, Transcriptional regulation of
955 pyruvate dehydrogenase kinase, Diabetes Metab. J. 36 (2012) 328–35.
956 doi:10.4093/dmj.2012.36.5.328.

957 [57] S. Zhang, M.W. Hulver, R.P. McMillan, M.A. Cline, E.R. Gilbert, The pivotal
958 role of pyruvate dehydrogenase kinases in metabolic flexibility, Nutr. Metab. 11
959 (2014) 10. doi:10.1186/1743-7075-11-10.

960 [58] B. Lindegaard, V.B. Mathews, C. Brandt, P. Hojman, T.L. Allen, E. Estevez,
961 M.J. Watt, C.R. Bruce, O.H. Mortensen, S. Syberg, C. Rudnika, J. Abildgaard, H.
962 Pilegaard, J. Hidalgo, S. Ditlevsen, T.J. Alsted, A.N. Madsen, B.K. Pedersen,
963 M.A. Febbraio, Interleukin-18 activates skeletal muscle AMPK and reduces
964 weight gain and insulin resistance in mice, Diabetes. 62 (2013) 3064–3074.
965 doi:10.2337/DB12-1095.

966 [59] P. Jiang, L. Ren, L. Zhi, Z. Yu, F. Lv, F. Xu, W. Peng, X. Bai, K. Cheng, L,
967 Quang, X. Zhang, X. Wang, Y. Zhang, D. Yang, X. Hu, R.P. Xiao, Negative
968 regulation of AMPK signaling by high glucose via E3 ubiquitin ligase MG53,
969 Mol. Cell. 81 (2021) 629-637.e5. doi:10.1016/J.MOLCEL.2020.12.008.

970 [60] C. Zhang, B. Zhang, X. Zhang, G. Sun, X. Sun, Targeting orphan nuclear
971 receptors NR4As for energy homeostasis and diabetes, Front. Pharmacol. 11
972 (2020) 587457. doi:10.3389/FPHAR.2020.587457.

973 [61] M.A. Pearen, J.M. Goode, R.L. Fitzsimmons, N.A. Eriksson, G.P. Thomas, G.J.

974 Cowin, S.C. Wang, Z.K. Tuong, G.E. Muscat, Transgenic muscle-specific Nor-1
975 expression regulates multiple pathways that effect adiposity, metabolism, and
976 endurance, Mol. Endocrinol. 27 (2013) 1897–1917. doi:10.1210/ME.2013-1205.
977 [62] S. Xu, H. Ni, H. Chen, Q. Dai, The interaction between STAT3 and nAChRα1
978 interferes with nicotine-induced atherosclerosis via Akt/mTOR signaling
979 cascade, Aging. 11 (2019) 8120–8138. doi:10.18632/AGING.102296.
980 [63] L. Zhang, Z. Chen, Y. Wang, D.J. Tweardy, W.E. Mitch, Stat3 activation induces
981 insulin resistance via a muscle-specific E3 ubiquitin ligase Fbxo40, Am. J.
982 Physiol. Endocrinol. Metab. 318 (2020) E625–E635.
983 doi:10.1152/AJPENDO.00480.2019.
984 [64] M.C. Monteiro, M. Sanyal, M.L. Cleary, C. Sengenès, A. Bouloumié, C. Dani, N.
985 Billon, PBX1: a novel stage-specific regulator of adipocyte development, Stem
986 Cells. 29 (2011) 1837–1848. doi:10.1002/STEM.737.
987 [65] D. Wu, D. Hu, H. Chen, G. Shi, I.S. Fetahu, F. Wu, K. Rabidou, R. Fang, L. Tan,
988 S. Xu, H. Liu, C. Argueta, L. Zhang, F. Mao, G. Yan, J. Chen, Z. Dong, R. Lv,
989 Y. Xu, M. Wang, Y. Ye, S. Zhang, D. Duquette, S. Geng, C. Yin, C.G. Lian, G.F.
990 Murphy, G.K. Adler, R. Garg, L. Lynch, P. Yang, Y. Li, F. Lan, J. Fan, Y. Shi,
991 Y.G. Shi, Glucose-regulated phosphorylation of TET2 by AMPK reveals a
992 pathway linking diabetes to cancer, Nature. 559 (2018) 637–641.
993 doi:10.1038/s41586-018-0350-5.
994 [66] T. Tamahara, K. Ochiai, A. Muto, Y. Kato, N. Sax, M. Matsumoto, T. Koseki, K.
995 Igarashi, The mTOR-Bach2 cascade controls cell cycle and class switch
996 recombination during B cell differentiation, Mol. Cell. Biol. 37 (2017) e00418-
997 17. doi:10.1128/MCB.00418-17.
998 [67] G. Leprivier, B. Rotblat, How does mTOR sense glucose starvation? AMPK is

the usual suspect, Cell Death Discov. 6 (2020) 27. doi:10.1038/S41420-020-0260-9.

[68] A. Itoh-Nakadai, M. Matsumoto, H. Kato, J. Sasaki, Y. Uehara, Y. Sato, R. Ebina-Shibuya, M. Morooka, R. Funayama, K. Nakayama, K. Ochiai, A. Muto, K. Igarashi, A Bach2-Cebp gene regulatory network for the commitment of multipotent hematopoietic progenitors, Cell Rep. 18 (2017) 2401–2414. doi:10.1016/J.CELREP.2017.02.029.

[69] K. Gopal, B. Saleme, R. Al Batran, H. Aburasayn, A. Eshreif, K.L. Ho, W.K. Ma, M. Almutairi, F. Eaton, M. Gandhi, E.A. Park, G. Sutendra, J.R. Ussher, FoxO1 regulates myocardial glucose oxidation rates via transcriptional control of pyruvate dehydrogenase kinase 4 expression, Am. J. Physiol. Circ. Physiol. 313 (2017) H479–H490. doi:10.1152/ajpheart.00191.2017.

[70] T. Glisovic, J.L. Bachorik, J. Yong, G. Dreyfuss, RNA-binding proteins and post-transcriptional gene regulation, FEBS Lett. 582 (2008) 1977–1986. doi:10.1016/J.FEBSLET.2008.03.004.

[71] B.S. Zhao, I.A. Roundtree, C. He, Post-transcriptional gene regulation by mRNA modifications, Nat. Rev. Mol. Cell Biol. 18 (2017) 31. doi:10.1038/NRM.2016.132.

[72] M.W. Hentze, A. Castello, T. Schwarzl, T. Preiss, A brave new world of RNA-binding proteins, Nat. Rev. Mol. Cell Biol. 19 (2018) 327–341. doi:10.1038/nrm.2017.130.

[73] Q. Sun, Q. Hao, K. V. Prasanth, Nuclear long noncoding RNAs: key regulators of gene expression, Trends Genet. 34 (2018) 142–157. doi:10.1016/J.TIG.2017.11.005.

[74] A. Velázquez-Cruz, B. Baños-Jaime, A. Díaz-Quintana, M.A.D. la Rosa, I. Díaz-

Moreno, Post-translational control of RNA-binding proteins and disease-related dysregulation, Front. Mol. Biosci. 8 (2021) 658852. doi:10.3389/FMOLB.2021.658852.

[75] M. Kubo, N. Ijichi, K. Ikeda, K. Horie-Inoue, S. Takeda, S. Inoue, Modulation of adipogenesis-related gene expression by estrogen-related receptor γ during adipocytic differentiation, Biochim. Biophys. Acta - Gene Regul. Mech. 1789 (2009) 71–77. doi:10.1016/J.BBAGRM.2008.08.012.

[76] B. Xiao, S.M. Gu, M.J. Li, J. Li, B. Tao, Y. Wang, Y. Wang, S. Zuo, Y. Shen, Y. Yu, D. Chen, G. Chen, D. Kong, J. Tang, Q. Liu, D.R. Cheng, Y. Liu, S. Alberti, M. Dovizio, R. Landolfi, L. Mucci, P.-Z. Miao, P. Gao, D.-L. Zhu, J. Wang, B. Li, P. Patrignani, Y. Yu, Rare SNP rs12731181 in the miR-590-3p target site of the Prostaglandin F2α receptor gene confers risk for essential hypertension in the Han Chinese population, Arterioscler. Thromb. Vasc. Biol. 35 (2015) 1687–1695. doi:10.1161/ATVBAHA.115.305445.

[77] Y. Wang, S. Yan, B. Xiao, S. Zuo, Q. Zhang, G. Chen, Y. Yu, D. Chen, Q. Liu, Y. Liu, Y. Shen, Y. Yu, Prostaglandin F 2α facilitates hepatic glucose production through CaMKIIγ/p38/FOXO1 signaling pathway in fasting and obesity, Diabetes. 67 (2018) 1748–1760. doi:10.2337/DB17-1521.

[78] P. Kaur, M.D. Reis, G.R. Couchman, S.N. Forjuoh, J.F. Greene, Jr, A. Asea, SERPINE 1 links obesity and diabetes: a pilot study, J. Proteomics Bioinform. 3 (2010) 191. doi:10.4172/JPB.1000139.

[79] G.M. Coudriet, J. Stoops, A.V. Orr, B. Bhushan, K. Koral, S. Lee, D.M. Previte, H.H. Dong, G.K. Michalopoulos, W.M. Mars, J.D. Piganelli, A Noncanonical role for plasminogen activator inhibitor type 1 in obesity-induced diabetes, Am. J. Pathol. 189 (2019) 1413–1422. doi:10.1016/J.AJPATH.2019.04.004.

1049 [80] C.-S. Kuo, J.-S. Chen, L.-Y. Lin, G.W. Schmid-Schönbein, S. Chien, P.-H.
1050 Huang, J.-W. Chen, S.-J. Lin, Inhibition of serine protease activity protects
1051 against high fat diet-induced inflammation and insulin resistance, Sci. Reports.
1052 10 (2020) 1–11. doi:10.1038/s41598-020-58361-4.
1053 [81] J. Kosacka, M. Nowicki, S. Paeschke, P. Baum, M. Blüher, N. Klö ting, Up-
1054 regulated autophagy: as a protective factor in adipose tissue of WOKW rats with
1055 metabolic syndrome, Diabetol. Metab. Syndr. 10 (2018) 13. doi:10.1186/S13098-
1056 018-0317-6.
1057 [82] J. Perttilä, K. Merikanto, J. Naukkarinen, I. Surakka, N.W. Martin, K.
1058 Tanhuanpää, V. Grimard, M.-R. Taskinen, C. Thiele, V. Salomaa, A. Jula, M.
1059 Perola, I. Virtanen, L. Peltonen, V.M. Olkkonen, OSBPL10, a novel candidate
1060 gene for high triglyceride trait in dyslipidemic Finnish subjects, regulates cellular
1061 lipid metabolism, J. Mol. Med. 2009 878. 87 (2009) 825–835.
1062 doi:10.1007/S00109-009-0490-Z.
1063 [83] R.F. Bowen, N.S. Raikwar, L.K. Olson, M.A. Deeg, Glucose and insulin regulate
1064 glycosylphosphatidylinositol-specific phospholipase D expression in islet beta
1065 cells, Metabolism. 50 (2001) 1489–1492. doi:10.1053/META.2001.28087.
1066 [84] S. Ussar, O. Bezy, M. Blüher, C.R. Kahn, Glypican-4 enhances insulin signaling
1067 via interaction with the insulin receptor and serves as a novel adipokine,
1068 Diabetes. 61 (2012) 2289–2298. doi:10.2337/DB11-1395.
1069 [85] W. Yang, T. Kelly, J. He, Genetic epidemiology of obesity, Epidemiol. Rev. 29
1070 (2007) 49–61. doi:10.1093/epirev/mxm004.
1071 [86] Y. Zhou, L. Rui, Leptin signaling and leptin resistance, Front. Med. 7 (2013)
1072 207–222. doi:10.1007/s11684-013-0263-5.
1073 [87] A.G. Izquierdo, A.B. Crujeiras, F.F. Casanueva, M.C. Carreira, Leptin, obesity,

and leptin resistance: where are we 25 years later?, Nutrients. 11 (2019) 2704. doi:10.3390/NU11112704.

Table 1: mRNA genes with the top 5% post-transcriptional signals (PTc) and reduced exonic fractions (ΔEx) > 2 folds (equivalent to -1 in the $\log_2$ scale) from *gluteus medius* skeletal muscle expression profiles of fasting (*AL-T0*, N = 11) and fed (*AL-T2*, N = 12) Duroc gilts.

ID	Gene	$\log_2$FC	ΔEx	PT_c	*P*-value	*q*-value	DE	miRNA target
ENSSSCG00000032094	*DKK2*	-2.010	-1.431	-4.738	1.654E-05	3.830E-03	•	x
ENSSSCG00000015334	*PDK4*	-2.108	-5.250	-4.698	4.693E-03	1.330E-01	x	x
ENSSSCG00000015037	*IL18*	-1.655	-1.191	-3.682	4.787E-03	1.340E-01	•	x
ENSSSCG00000005385	*NR4A3*	-1.337	-3.082	-3.646	4.038E-02	4.098E-01	x	x
ENSSSCG00000003766	*DNAJB4*	-1.391	-1.008	-3.348	8.358E-03	1.905E-01		x
ENSSSCG00000015969	*CHRNA1*	-1.561	-1.339	-3.341	2.606E-03	9.406E-02	x	x
ENSSSCG00000039419	*SLCO4A1*	-1.055	-2.279	-3.180	2.820E-02	3.544E-01	x	x
ENSSSCG00000049158		-1.107	-1.096	-3.164	3.182E-02	3.735E-01		x
ENSSSCG00000004347	*FBXL4*	-1.298	-1.126	-3.133	1.422E-03	6.520E-02	x	x
ENSSSCG00000004979	*MYO9A*	-1.239	-1.003	-3.043	7.296E-03	1.731E-01		x
ENSSSCG00000013351	*NAV2*	-1.163	-1.196	-2.863	2.605E-04	2.301E-02	x	x
ENSSSCG00000032741	*TBC1D9*	-0.913	-1.061	-2.736	1.534E-02	2.583E-01	•	x
ENSSSCG00000031728	*ABRA*	-1.238	-1.393	-2.704	1.295E-03	6.116E-02	x	x
ENSSSCG00000006331	*PBX1*	-0.891	-1.039	-2.480	1.135E-02	2.177E-01	x	x
ENSSSCG00000035037	*SIK1*	-1.357	-1.289	-2.475	3.999E-03	1.212E-01	x	x
ENSSSCG00000038374	*CIART*	-1.027	-1.321	-2.052	1.543E-02	2.587E-01	x	
ENSSSCG00000023806	*LRRN1*	-0.776	-1.013	-1.983	1.580E-01	7.074E-01		x
ENSSSCG00000009157	*TET2*	-0.381	-1.123	-1.792	4.880E-01	9.582E-01		x
ENSSSCG00000011133	*PFKFB3*	-0.022	-2.256	-1.785	9.712E-01	9.987E-01	x	x
ENSSSCG00000002283	*FUT8*	-0.578	-1.286	-1.784	9.887E-02	6.059E-01	x	x
ENSSSCG00000023133	*OSBPL6*	-0.432	-1.088	-1.772	3.835E-01	9.108E-01	x	
ENSSSCG00000017986	*NDEL1*	-0.767	-1.644	-1.759	1.006E-02	2.081E-01	x	x
ENSSSCG00000031321	*NR4A1*	-0.630	-1.328	-1.720	6.298E-02	5.006E-01	x	
ENSSSCG00000035101	*KLF5*	-0.519	-1.487	-1.708	2.942E-01	8.488E-01	x	x
ENSSSCG00000004332	*BACH2*	-0.714	-2.105	-1.705	9.089E-02	5.861E-01	x	x
ENSSSCG00000017983	*PER1*	-0.773	-1.073	-1.627	3.000E-02	3.662E-01	x	

[a]Log_2FC: estimated $\log_2$ fold change for mean exonic fractions from *gluteus medius* expression profiles of fasted *AL-T0* and fed *AL-T2* Duroc gilts; [b]ΔEx: exonic fraction increment ($Ex_2 - Ex_1$) when comparing exon abundances in *AL-T0* (Ex_1) vs *AL-T2* (Ex_2) Duroc gilts; [c]PTc: post-transcriptional signal (ΔEx – ΔInt) in z-score scale; [d]q-value: q-value calculated with the false discovery rate (FDR) approach [32]. The "x" symbols represent differentially expressed (DE) genes (FC < -2; *q*-value < 0.05) according to their exonic fractions, as well as those targeted by at least one of the upregulated miRNAs excluding redundant seeds (N = 6, **Table S5**). The "•" symbol represents suggestive canonical differential expression (*P*-value < 0.01, **Table S4**).

Table 2: mRNA genes with the top 5% post-transcriptional signals (PTc) and reduced exonic fractions (ΔEx) > 3 folds (equivalent to -1.58 in the $\log_2$ scale) from adipocyte expression profiles of *lean* (N = 5) and *obese* (N = 5) Duroc-Göttingen minipigs according to their body mass index (BMI).

mRNA	Gene	$\log_2$FC[a]	ΔEx[b]	PTc[c]	*P*-value	*q*-value[d]	DE	miRNA target
ENSSSCG00000010814	*ESRRG*	-0.591	-5.305	-6.425	7.364E-01	9.996E-01		x
ENSSSCG00000032452	*WFS1*	-2.198	-2.138	-5.510	9.509E-03	9.996E-01	x	
ENSSSCG00000039548	*PTGFR*	-1.634	-1.590	-4.915	8.804E-03	9.996E-01	•	x
ENSSSCG00000002265	*FAM174B*	-1.244	-1.726	-4.179	5.385E-02	9.996E-01	•	x
ENSSSCG00000016233	*SERPINE2**	-1.735	-2.060	-3.603	5.684E-02	9.996E-01	x	x
ENSSSCG00000006243	*PENK*	-0.42	-2.104	-3.573	7.628E-01	9.996E-01		
ENSSSCG00000014921	*PRSS23**	-1.141	-1.739	-3.360	2.719E-01	9.996E-01	•	x
ENSSSCG00000017186	*RNF157**	-1.218	-2.338	-3.317	2.413E-01	9.996E-01	x	x
ENSSSCG00000031819	*TP53I11*	-1.002	-1.711	-2.883	4.102E-01	9.996E-01		x
ENSSSCG00000001089	*GPLD1*	-0.872	-1.761	-2.723	4.302E-01	9.996E-01		x
ENSSSCG00000003377	*ACOT7*	-0.79	-2.688	-2.544	3.439E-01	9.996E-01	x	
ENSSSCG00000040464	*LEP**	-0.747	-2.186	-2.463	1.880E-01	9.996E-01	x	x
ENSSSCG00000025652	*CDH1*	-0.472	-2.592	-2.372	6.533E-01	9.996E-01	•	x
ENSSSCG00000011230	*OSBPL10**	-0.576	-1.594	-1.869	4.272E-01	9.996E-01	•	x
ENSSSCG00000017328	*ARHGAP27*	-0.235	-2.788	-1.699	8.113E-01	9.996E-01	x	x

[a]$\log_2$FC: estimated $\log_2$ fold change for mean exonic fractions from adipocyte expression profiles of *lean* and *obese* Duroc-Göttingen minipigs; [b]ΔEx: exonic fraction increment ($Ex_2 - Ex_1$) when comparing exon abundances in *obese* (Ex_1) vs *lean* (Ex_2) Duroc gilts; [c]PTc: post-transcriptional signal (ΔEx – ΔInt) in z-score scale; [d]*q*-value: *q*-value calculated with the false discovery rate (FDR) approach [32]. The "x" symbols represent differentially expressed (DE) genes (FC < -2; *q*-value < 0.05) according to their exonic fractions, as well as those targeted by at least one of the upregulated miRNAs excluding redundant seeds (N = 4, **Table S10**). The "•" symbol represents suggestive canonical differential expression (*P*-value < 0.01, **Table S9**).

Figure legends

Figure 1: (**A**) Scatterplot depicting mRNA genes with the top 5% negative post-transcriptional regulatory signals according to exonic (ΔEx) and PTc (ΔEx – ΔInt) scores (in purple) and putatively targeted by upregulated (FC > 1.5; *q*-value < 0.05) miRNAs from *gluteus medius* skeletal muscle expression profiles of fasted (*AL-T0*, N = 11) and fed (*AL-T2*, N = 12) Duroc gilts. (**B**) Enrichment analyses of the number of mRNA genes with the top 5% negative post-transcriptional signals (PTc) and reduced exonic fractions (ΔEx) > 2 folds putatively targeted by DE upregulated miRNAs (FC > 1.5; *q*-value < 0.05), DE downregulated miRNAs (FC < -1.5; *q*-value < 0.05) and the top 5% most highly expressed miRNAs excluding DE upregulated miRNAs. (**C**) Scatterplot depicting DE upregulated (in green) and downregulated (in red) mRNA genes (|FC| > 2; *q*-value < 0.05) according to exonic (ΔEx) and PTc (ΔEx – ΔInt) scores. (**D**) Enrichment analyses considering DE downregulated mRNA genes (FC < -2; *q*-value < 0.05) and excluding those with the top 5% putative post-transcriptional regulatory signals previously analyzed. The black dashed line represents a *P*-value = 0.05.

Figure 2: (**A**) Scatterplot depicting mRNA genes with the top 5% negative post-transcriptional regulatory signals according to exonic (ΔEx) and PTc (ΔEx – ΔInt) scores (in purple) and putatively targeted by upregulated (FC > 1.5; *P*-value < 0.01) miRNAs from adipocyte expression profiles of *lean* (N = 5) and *obese* (N = 5) Duroc-Göttingen minipigs according to their body mass index (BMI). (**B**) Enrichment analyses of the number of mRNA genes with the top 5% negative post-transcriptional signals (PTc) and reduced exonic fractions (ΔEx) > 3 folds (equivalent to 1.58 in the $\log_2$ scale) putatively targeted by DE upregulated miRNAs (FC > 1.5; *P*-value < 0.01), DE

downregulated miRNAs (FC < -1.5; *P*-value < 0.01) and the top 5% most highly expressed miRNAs excluding DE upregulated miRNAs. (**C**) Barplots depicting qPCR log_2 transformed relative quantities (Rq) for *LEP, OSBPL10, PRSS23, RNF157* and *SERPINE2* mRNA transcripts measured in adipocytes from the retroperitoneal fat of *lean* (N = 5) and *obese* (N = 5) Duroc-Göttingen minipigs. (**D**) Barplots depicting qPCR log_2 transformed relative quantities (Rq) for ssc-miR-148a-3p, ssc-miR-214-3p and ssc-miR-92b-3p miRNA transcripts measured in the isolated adipocytes from the retroperitoneal fat of *lean* (N = 5) and *obese* (N = 5) Duroc-Göttingen minipigs.

Figure 3: Covariation enrichment scores (CES) for the exonic and intronic fractions of mRNA genes with post-transcriptional signals (PTc) and putatively targeted by upregulated miRNAs from (**A**) *gluteus medius* skeletal muscle expression profiles of fasted (*AL-T0*, N = 11) and fed (*AL-T2*, N = 12) Duroc gilts and (**B**) adipocyte expression profiles of *lean* (N = 5) and *obese* (N = 5) Duroc-Göttingen minipigs according to their body mass index (BMI). The top post-transcriptional signals were defined as the 5% most negative PTc scores and reduced exonic fractions (ΔEx) > 2 folds for *AL-T0* vs *ALT-2* Duroc gilts (N = 21) and (ΔEx) > 3 folds for *lean* vs *obese* Duroc-Göttingen minipigs (N = 12), respectively. The control set of CES values were generated by permuted (N = 1,000) random sets of exonic and intronic profiles of genes with same length as those with post-transcriptional signals in both contrasts (N = 21 for *AL-T0* vs *ALT-2* and N = 12 for *lean* vs *obese*). Significant differences were assessed using a Mann-Whitney U non-parametric test [40].

Supplementary Tables

Table S1: Phenotype values for selected Duroc-Göttingen minipigs from the F2-UNIK source population according to their body mass indexes (BMI).

Table S2: Primers for qPCR validation of selected mRNA and miRNA genes according to EISA results in the F2-UNIK Duroc-Göttingen minipig population comparing *lean* (N = 5) and *obese* (N = 5) individuals.

Table S3: Raw Cq values after efficiency correction measuring adipocyte expression profiles of selected mRNAs and miRNAs from *lean* (N = 5) and *obese* (N = 5) Duroc-Göttingen minipigs.

Table S4: Genes detected by *edgeR* tool as differentially expressed when comparing *gluteus medius* expression profiles of fasted *AL-T0* (N = 11) and fed *AL-T2* (N = 12) Duroc gilts.

Table S5: microRNA genes detected by *edgeR* tool as differentially expressed when comparing *gluteus medius* expression profiles of fasted *AL-T0* (N = 11) and fed *AL-T2* (N = 12) Duroc gilts.

Table S6: EISA analyses for post-transcriptional signals detected in *gluteus medius* skeletal muscle expression profiles of fasted (*AL-T0*, N = 11) and fed (*AL-T2*, N = 12) Duroc gilts.

Table S7: Binding sites for differentially upregulated miRNAs from mRNA genes with the top 5% negative PTc scores and reduced ΔEx > 2 folds from *gluteus medius* skeletal muscle expression profiles of fasting (*AL-T0*, N = 11) and fed (*AL-T2*, N = 12) Duroc gilts.

Table S8: Binding sites for differentially upregulated miRNAs from the 5'-UTR of the two transcripts annotated for the ENSSSCG00000049158 mRNA gene.

Table S9: Genes detected by *edgeR* tool as differentially expressed when comparing adipocyte expression profiles from *lean* (N = 5) and *obese* (N = 5) Duroc-Göttingen minipigs according to their body mass index (BMI).

Table S10: microRNA genes detected by *edgeR* tool as differentially expressed when comparing adipocyte expression profiles from *lean* (N = 5) and *obese* (N = 5) Duroc-Göttingen minipigs according to their body mass index (BMI).

Table S11: Genes with the top 5% post-transcriptional signals (PTc) and reduced exonic fractions (ΔEx) > 3 folds (equivalent to -1.58 in the $\log_2$ scale) from adipocyte expression profiles of *lean* (N = 5) and *obese* (N = 5) Duroc-Göttingen minipigs according to their body mass index (BMI).

Table S12: Binding sites for differentially upregulated miRNAs from mRNA genes with top 5% negative PTc scores and reduced ΔEx > 3 folds from adipocyte expression profiles of *lean* (N = 5) and *obese* (N = 5) Duroc-Göttingen minipigs according to their body mass index (BMI).

Table S13: Covariation enrichment scores (CES) for the exonic and intronic fractions of mRNA genes with the top 5% post-transcriptional signals (PTc) that were putatively targeted by DE upregulated miRNAs from *gluteus medius* skeletal muscle expression profiles *AL-T0* vs *AL-T2* Duroc gilts (N = 21), as well as from adipocyte expression profiles of *lean* vs *obese* Duroc-Göttingen minipigs (N = 12).

Supplementary Figures

Figure S1: (**A**) Scatterplot depicting post-transcriptional regulatory signals according to differences in the exonic fraction (ΔEx) and PTc (ΔEx – ΔInt) scores. (**B**) The classification and interpretation of post-transcriptional signals according to ΔEx, ΔInt (Tc) and ΔEx - ΔInt (PTc) values. (**C**) Diagram depicting the consecutive steps implemented for studying miRNA-driven post-transcriptional regulatory signals applying the EISA approach and additional enrichment and covariation analyses.

Figure S2: Scatterplots depicting the exonic (ΔEx) and intronic (ΔInt) fractions from *gluteus medius* skeletal muscle expression profiles of fasting (*AL-T0*, N = 11) and fed (*AL-T2*, N = 12) Duroc gilts. (**A**) mRNA genes with the top 5% post-transcriptional (PTc) negative scores and reduced exonic (ΔEx) fractions > 2 folds (equivalent to -1 in the $\log_2$ scale), suggestive of miRNA-driven post-transcriptional regulation. (**B**) mRNA genes differentially expressed showing upregulation (FC > 2; *q*-value < 0.05, in green) and downregulation (FC < -2, *q*-value < 0.05, in red) in fed (*AL-T2*, N = 12) Duroc gilts with respect to their fasted (*AL-T0*, N = 11) counterparts.

Figure S3: Enrichment analyses of the number of genes with the (**A**) top 1% and (**B**) top 5% negative post-transcriptional signals (PTc) and reduced exonic fractions (ΔEx) > 2 folds putatively targeted by upregulated miRNAs (FC > 1.5; *q*-value < 0.05) from *gluteus medius* skeletal muscle expression profiles of fasting (*AL-T0*, N = 11) and fed (*AL-T2*, N = 12) Duroc gilts and the consequences of incorporating context-based pruning of miRNA binding sites of type 8mer, 7mer-m8 and 7mer-A1. R: Raw enrichment analyses without any additional context-based pruning. AU: Enrichment analyses removing miRNA binding sites without AU-rich flanking sequences (30 nts upstream and downstream). M: Enrichment analyses removing miRNA binding sites located in the middle of the 3'-UTR sequence (45-55%). E: Enrichment analyses removing miRNA binding sites located too close (< 15 nts) to the beginning or the end of the 3'-UTR sequences. The black dashed line represents a *P*-value = 0.05.

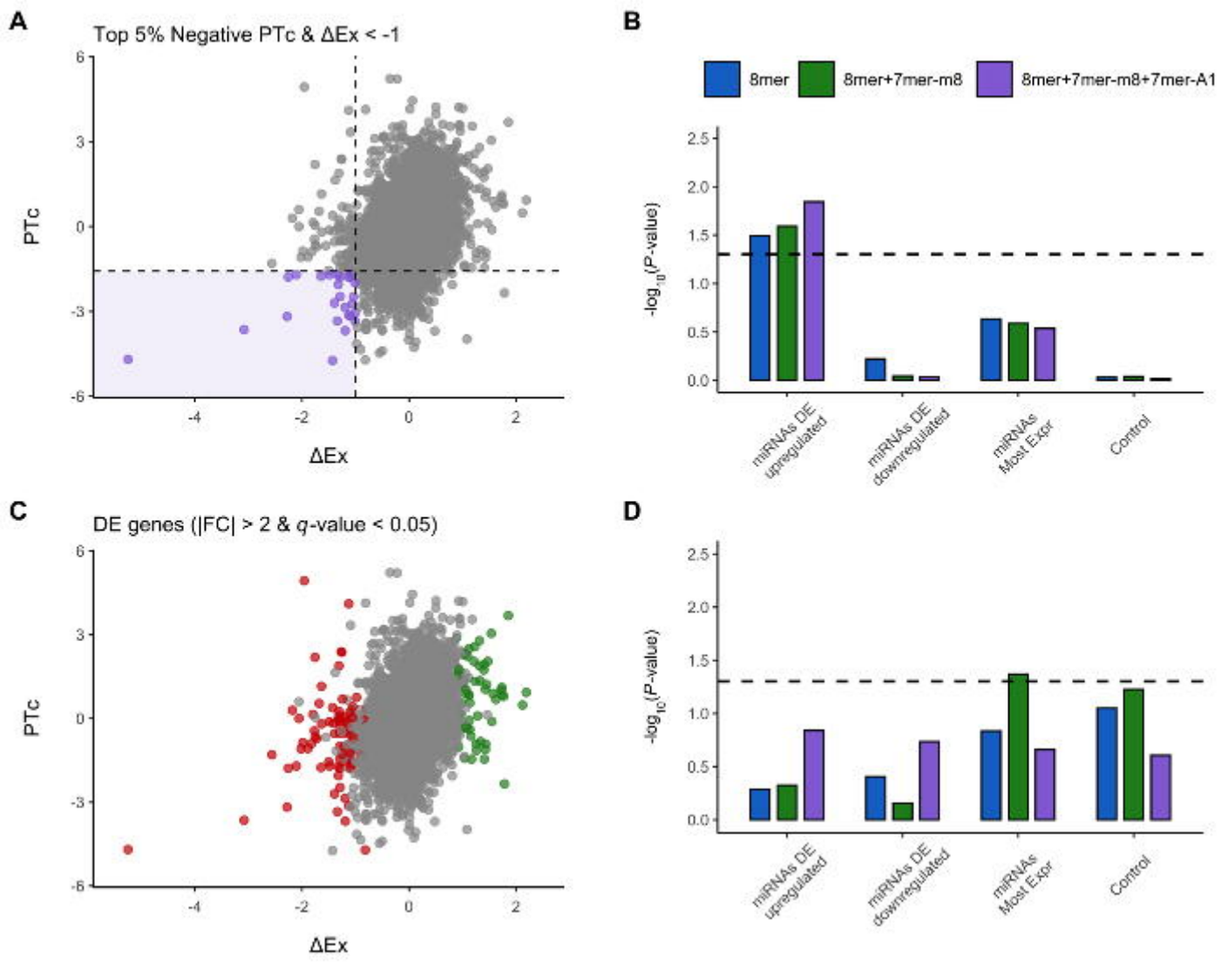
A
Top 5% Negative PTc & ΔEx < -1
PTc
ΔEx
B
8mer
8mer+7mer-m8
8mer+7mer-m8+7mer-A1
-log10(P-value)
miRNAs DE upregulated
miRNAs DE downregulated
miRNAs Most Expr
Control
C
DE genes (|FC| > 2 & q-value < 0.05)
PTc
ΔEx
D
-log10(P-value)
miRNAs DE upregulated
miRNAs DE downregulated
miRNAs Most Expr
Control

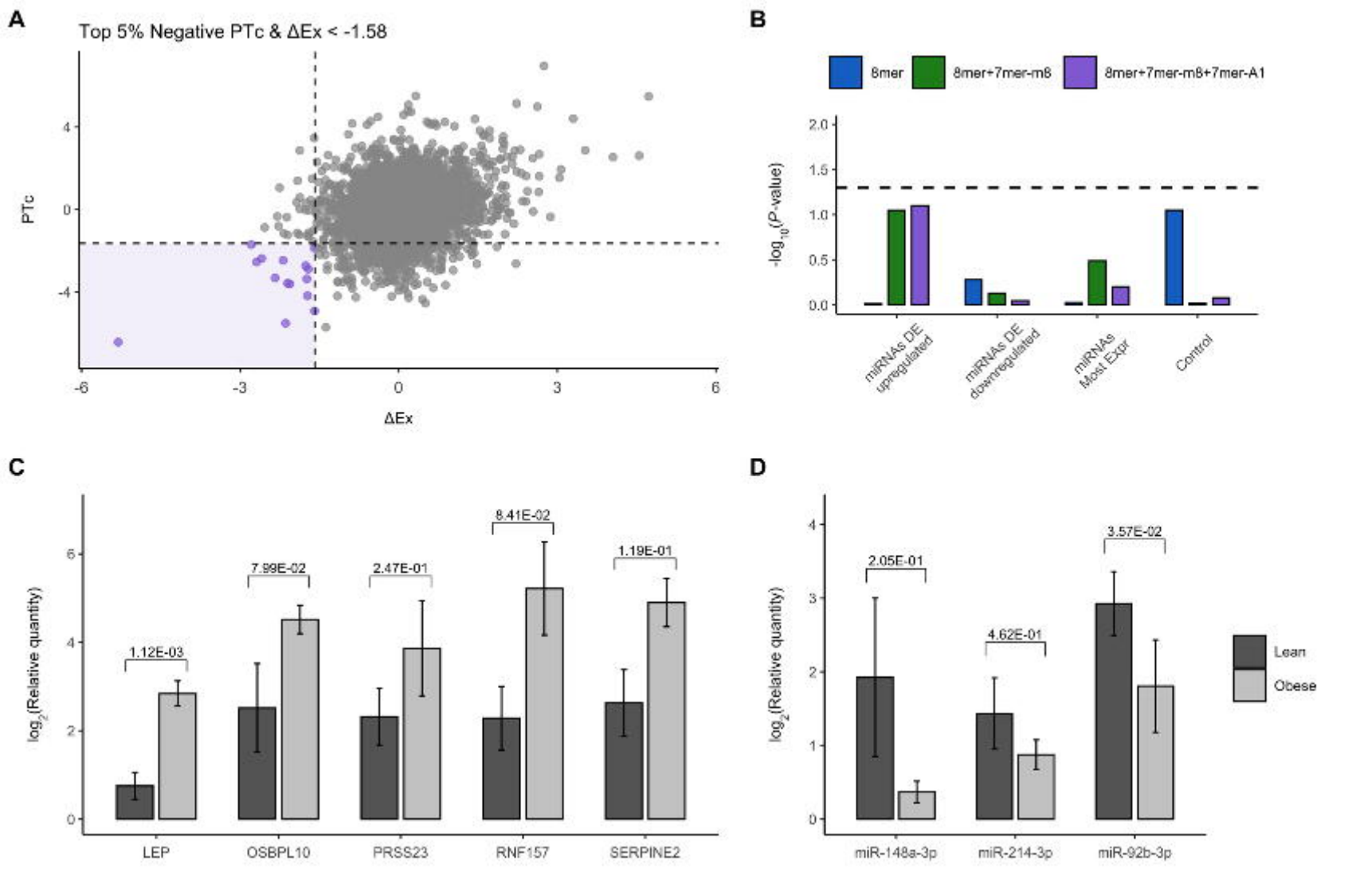
A
Top 5% Negative PTc & ΔEx < -1.58
PTc
ΔEx
B
8mer
8mer+7mer-m8
8mer+7mer-m8+7mer-A1
-log10(P-value)
miRNAs DE upregulated
miRNAs DE downregulated
miRNAs Most Expr
Control
C
log2(Relative quantity)
1.12E-03
7.99E-02
2.47E-01
8.41E-02
1.19E-01
LEP
OSBPL10
PRSS23
RNF157
SERPINE2
D
log2(Relative quantity)
2.05E-01
4.62E-01
3.57E-02
miR-148a-3p
miR-214-3p
miR-92b-3p
Lean
Obese

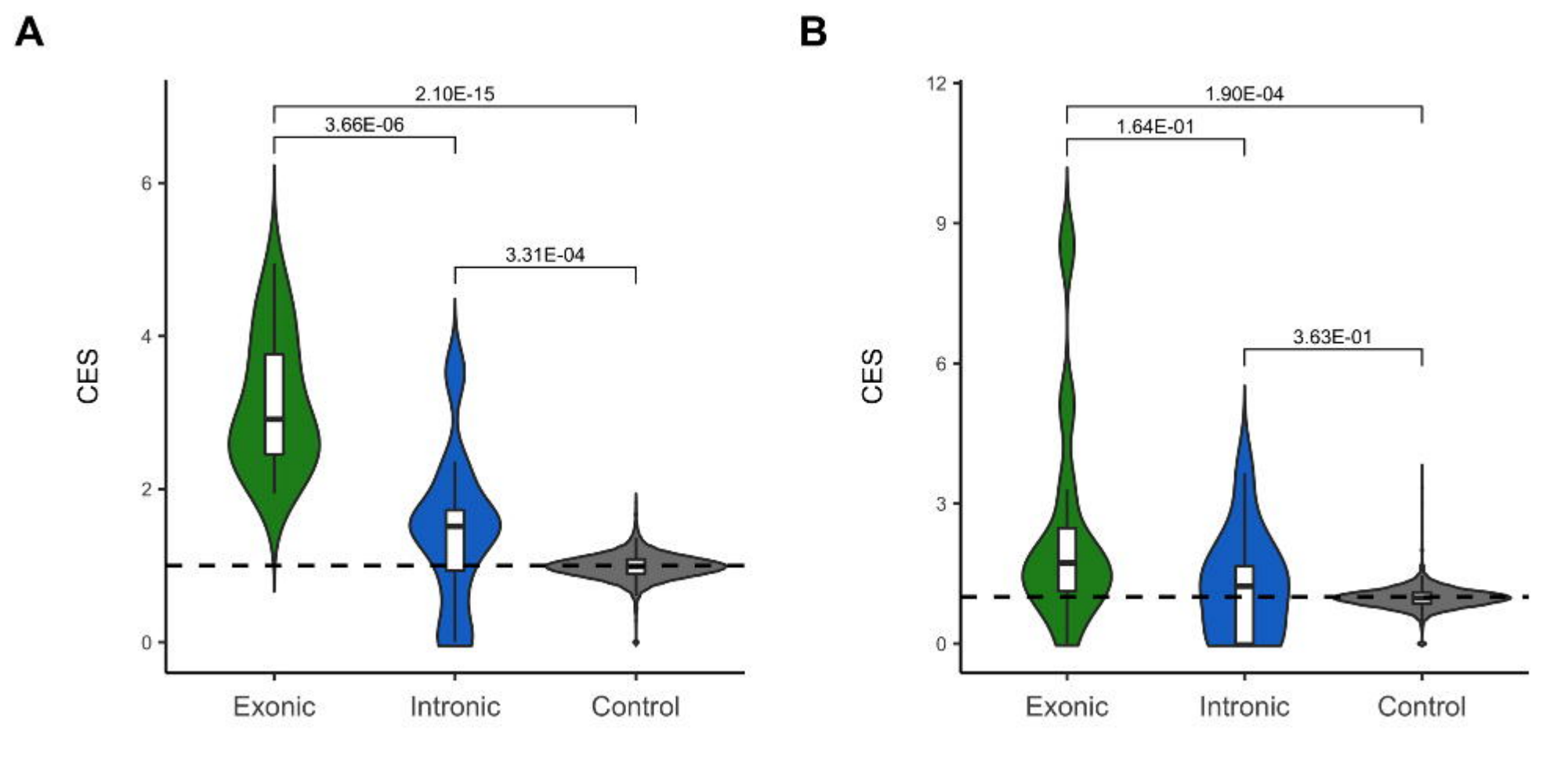
A
2.10E-15
3.66E-06
3.31E-04
CES
0
2
4
6
Exonic
Intronic
Control
B
1.90E-04
1.64E-01
3.63E-01
CES
0
3
6
9
12
Exonic
Intronic
Control